MAYFLOWER WIND

Appendix F1. Sediment Plume Impacts from Construction Activities

Document Revision A

Issue Date February 2021

Final Sediment Plume Impacts from Construction Activities

Mayflower Wind Energy LLC | USA

C170693-02 05 | 8 February 2021
Final Report
AECOM

Document Control

Document Information

Project Title	Mayflower Wind Energy LLC
Document Title	Final Sediment Plume Impacts from Construction Activities
Fugro Project No.	C170693
Fugro Document No.	C170693-02
Issue Number	05
Issue Status	Final Report
Fugro Legal Entity	Fugro USA Marine Inc.
Issuing Office Address	6100 Hillcroft Ave, Houston, TX 77081, USA

Client Information

Client	AECOM
Client Address	9 Jonathan Bourne Drive, Pocasset, MA 02559
Client Contact	Nancy Palmstrom
Client Document No.	F1

Document History

Issue	Date	Status	Comments on Content	Prepared By	Checked By	Approved By
0	08 February 2021		Final Report	SBL/BSP/RVS	BSP	RVS

Project Team

Initials	Name	Role
BSP	Benoit Spinewine, PhD	Principal Engineer, Project Manager
SBL	Sébastien Blaise, PhD	Senior Engineer
RVS	Rafael V. Schiller, PhD	Metocean Consultancy Manager, Americas

FUGRO
Fugro USA Marine Inc.
6100 Hillcroft Ave
Houston, TX 77081
USA

AECOM
Attn: Nancy Palmstrom
9 Jonathan Bourne Drive
Pocasset, MA 02559
United States of America

8 February 2021

Dear Madam,

We have the pleasure to submit to you our final report for the assessment of sediment plume impacts from construction activities related to the Mayflower Wind Project. The report presents the input, methodology and results of our study with the objective of assessing the impact of sediment dispersion associated with the installation of the offshore export cables and inter-array cables. Please do not hesitate to contact us should you have any question regarding this report.

Yours faithfully,

Benoit Spinewine
Principal Engineer

Executive Summary

Mayflower Wind Energy LLC (Mayflower Wind) proposes an offshore wind renewable energy generation project (Project) located in federal waters off the southern coast of Massachusetts in the Outer Continental Shelf (OCS) Lease Area OCS-A 0521. The Project will deliver electricity to the regionally administered transmission system via export cables with a landing location in Falmouth, Massachusetts.

Mayflower Wind's construction and installation concept includes wind turbine generators (WTGs), offshore substation platform(s) (OSP(s)), inter-array cables, and offshore export cables. Cable installation, involving trenching, dredging, and nearshore horizontal directional drilling (HDD), will result in seabed disturbance, including suspension of sediment in the water column, and subsequent redeposition of sediments on the seabed. In alignment with the Bureau of Ocean Energy Management (BOEM) guidelines, for the Construction and Operations Plan (COP) (BOEM, 2020), this study addresses the following:

- Quantify concentrations of sediment suspended in the water column (as total suspended solids) following seafloor disturbance during cable installation
- Quantify the extent and thickness of sediment re-deposited to the seafloor following suspension.

A high-resolution, site-specific wave and current model was developed to simulate the metocean conditions over the Lease Area and offshore export cable corridors. The model was verified and validated against site-specific measurements and then applied to drive scenarios of the sediment plume dispersion from trenching and dredging activities.

The redeposition of the sediment occurs relatively locally. Most of the released mass settles out quickly and is not transported for long by the currents. Deposition thicknesses exceeding 5 mm (0.20 inch) are generally limited to a corridor of maximum width 24 m (79 ft) around the cable route, although such thicknesses can be locally observed up to 180 m (590 ft) from the cable route. A thicker layer of deposits over a smaller area tends to be observed in the vicinity of the deeper section called "Segment 3" (KP 45 to KP 88) of the export cables and in the vicinity of the inter-array cables, which is the consequence of the lower currents present in these areas resulting in less transport of sediment away from the cable installation site.

Dredging at the HDD exit pit is expected to have very limited impacts in terms of deposited sediment, with deposits exceeding 5 mm (0.20 inch) thickness found at respective maximum distances of 26 m and 32 m (85 ft and 105 ft) for the Neap and Spring Tide scenarios. However, in very close proximity to the HDD exit pit, the thickness of deposits exceeds 0.1 m (0.3 ft). Deposition thicknesses are greater if the location of the release is fixed. Cable trenching or dredging operations are mobile, and thus will produce smaller maximum deposit thicknesses.

The observations of maximum Total Suspended Solids (TSS) are correlated with the thickness of the deposits. Concentrations above 100 mg/l (0.0008 lb/gal) generally remain suspended around the

route centerline. They are predicted to extend to a maximum of 370 m (1,214 ft) from the cable route centerlines and affect a cumulative area of 1,849 ha (4,569 acres) for the entirety of the export cable and inter-array cable routes. Further, the 150 mg/L (0.0013 lb/gal) contour is always within 250 m (820 ft) from the centerline. Observations of significant sediment concentrations exceeding 50 mg/l (0.00042 lb/gal) are generally limited to the first 5 m (16 ft) above the seabed, although they can attain 10 m (16 ft) above seabed in the case of the inter-array cables.

Turbidity levels associated with the HDD exit pit dredging are significantly smaller compared with the impact resulting from cable trenching or dredging, with concentrations exceeding 100 mg/l (0.0008 lb/gal) found at a maximum distance of 36 m (118 ft) and affecting a cumulative area not exceeding 0.4 ha (1 acre).

The maximum TSS level drops below 10 mg/l (0.00008 lb/gal) in two hours for any of the simulated scenarios, while it drops below 1 mg/l (0.000008 lb/gal) after less than four hours.

In summary, seabed deposits and water quality impacts from cable installation and HDD exit pit dredging remain generally localized and of short duration.

Contents

Attachments

Figures in the Main Text

Tables in the Main Text

Abbreviations and Acronyms

ac	Acre(s)
BOEM	Bureau of Ocean Energy Management
CFR	Code of Federal Regulation
COP	Construction and Operations Plan
ft	Foot/feet
gpm	Gallons per minute
ha	Hectare(s)
HDD	Horizontal Directional Drilling
Hs	Significant wave height
HYCOM NCODA	Hybrid Coordinate Ocean Model Navy Coupled Ocean Data Assimilation
km	Kilometer(s)
KP	Kilometer Point
lb/gal	Pounds per gallon
LiDAR	Light Detection And Ranging
m	Meter(s)
mi	Statute mile(s)
MLLW	Mean Lower Low Water
m^3/hr	Cubic meters per hour
mm	millimeter
mi/hr	Miles per hour
m/s	Meters per second
mg/l	Milligrams per liter
NCEP CFSR	National Centers for Environmental Prediction Climate Forecast System Reanalysis
nm	Nautical mile(s)
N/m^2	Newtons per meter squared
OCS	Outer Continental Shelf
OSP(s)	Offshore Substation Platform(s)
PSD	Particle Size Distribution
QQ	Quantile-Quantile
ROMS	Regional Ocean Modelling System
ROV	Remotely Operated Vehicle
SWAN	Simulating Waves Nearshore
Tp	Peak wave period
TSS	Total Suspended Solids
WTG	Wind Turbine Generator

1 Introduction

Mayflower Wind Energy LLC (Mayflower Wind) proposes an offshore wind renewable energy generation project (Project) located in federal waters off the southern coast of Massachusetts in the Outer Continental Shelf (OCS) Lease Area OCS-A 0521 (Lease Area) which will deliver electricity to the regionally administered transmission system via offshore export cables that will make landfall in Falmouth, Massachusetts.

This report presents an assessment of sediment plume dispersion (deposits and Total Suspended Solids [TSS]) associated with installation of the inter-array cables within the Lease Area, the export cables between the Lease Area and landing(s), and the nearshore HDD entry point for subsurface cable installation for the shoreline landing.

The remainder of this section articulates the assessment objectives, provides a Project overview, describes the report organization, and summarizes units and conventions used throughout the balance of the report.

1.1 Assessment Objectives

The Bureau of Ocean Energy Management (BOEM) produced regulations and guidelines for preparing a COP and conducting specific technical studies to support COP development. Consistent with BOEM's Information Guidelines for a Renewable Energy Construction and Operations Plan (COP) (BOEM, 2020), the objectives of this sediment plume dispersion assessment are to:

- Model disturbances associated with cable installation, including near shore HDD entry, and specifically the resulting:
  - Suspended sediments in the water column (TSS)
  - Redeposition of disturbed and suspended sediments including thickness and extent on the seabed

Results from the sediment plume dispersion assessment provide quantitative and qualitative information to support the Mayflower Wind COP.

1.2 Project Overview

The Lease Area is located offshore of the southern coast of Massachusetts, approximately 49 kilometers (km) [26 nautical miles (nm)] south of Martha's Vineyard and 37 km (20 nm) south of Nantucket (Figure 1.1).

The Project layout will align to a 1 nm x 1 nm grid with an east-west and north-south orientation, as agreed upon across the entire Massachusetts/Rhode Island (MA/RI) Wind Energy Areas. The Project will consist of up to 149 positions within the Lease Area, to be occupied by WTGs and OSP(s), connected with inter-array cables.

For purposes of this modelling effort, water depths were estimated based on preliminary information. Within the Lease Area, these range from approximately 37 m (121 ft) to 64 m (210 ft), with deeper waters located in the southwest. The average depth is 51 m (167 ft). The submarine offshore export cables will travel from one or more OSP(s) within the Lease Area through Muskeget Channel into Nantucket Sound and arrive at landing location(s) in Falmouth, MA. The cables are planned to be buried along the route. The three potential landfall sites, from west to east, include locations at the end of Mill Road (alternate), Shore Street (alternate), and Worcester Avenue (preferred).

Additional details regarding the Project description and construction and installation methods are available in Section 3 of the COP. Specific details regarding construction methods used in this assessment are provided in Section 2 of this report.

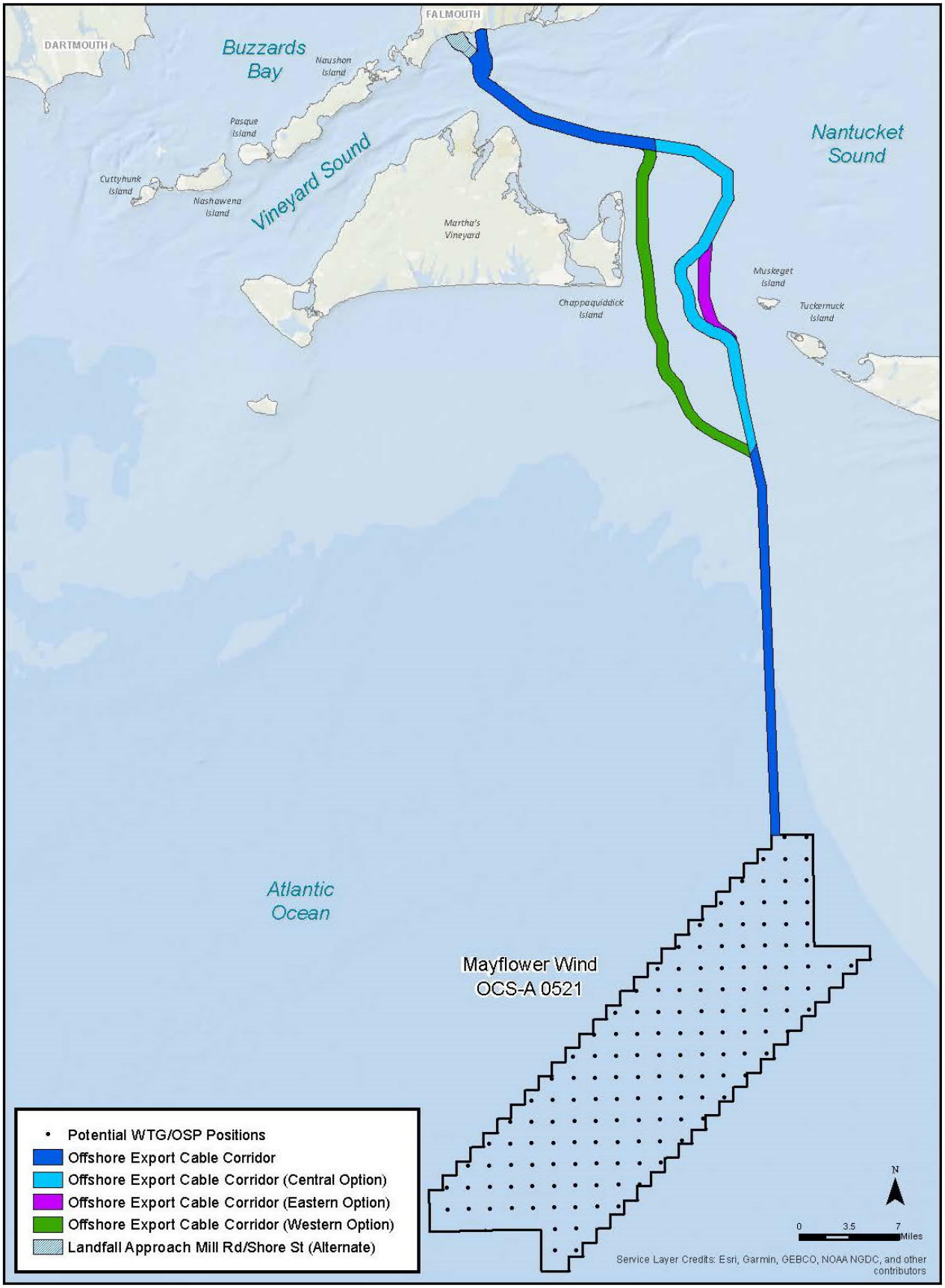

Figure 1.1. Location of the Mayflower Wind Project.

1.3 Report Organization

This report includes:

- A presentation of the construction and design scenarios to be evaluated (Section 2)
- The development of the wave/current model that drives the suspended plume dispersion simulations (Section 3)
- A presentation of the sediment plume dispersion model tool (Section 4)
- A presentation and discussion of the results (Section 5 for deposits, Section 6 for maximum TSS, Section 7 for impact duration)
- Conclusions and considerations about the sediment plume impact for different scenarios and locations (Section 8)
- References (Section 9)
- Details on the data sources (Attachment A)
- Details on the metocean modelling methodology (Attachment B)
- Details on the sediment plume modelling methodology (Attachment C)

1.4 Units and Conventions

The following list describes the units and conventions used in this report.

- Significant wave height (Hs) is expressed in meters [m]
- Peak wave period (Tp) is expressed in seconds [s]
- Wave direction is expressed in compass points or degrees, measured clockwise from true north, and describes the direction from which the waves were travelling
- Current speed is expressed in meters per second [m/s] at depth [m] below mean sea level
- Current direction is expressed in compass points or degrees, measured clockwise from true north, and describes the direction towards which the currents were flowing
- Wind stress in expressed in Newtons per meter squared [N/m^2]
- Vertical elevations in the water column are expressed in meters. Depths are quoted below Mean Lower Low Water (MLLW) and heights are quoted above seabed
- Distances are expressed in kilometers [km] except where stated otherwise
- Sediment grain sizes are expressed in millimeters [mm] except where stated otherwise
- Sediment thicknesses of deposits are expressed in millimeter [mm]
- Sediment concentrations (TSS) are expressed in milligrams per liter [mg/l]
- Surfaces impacted by sediment are expressed in hectare [ha] except where stated otherwise

2 Construction Scenarios

This section describes the cable installation scenarios that are being evaluated as part of the Mayflower Wind Project. Modelling assumptions in terms of the construction activities, characteristics of the sediment plume source, metocean conditions, and number of simulations are presented below.

The advance rate for each scenario corresponds to an average rate based upon the considered cable installation methods. The duration for each scenario is based upon a total length divided by the assumed advance rate.

The simulation scenarios consider a single cable corridor for the offshore export cables and a single route for the inter-array cables. These were chosen to be representative of the different options including the range of water depths and locations susceptible to be encountered. Several cables installed in sequence would not result in increased turbidity levels, but associated deposits would be additive in areas of overlapping plumes.

2.1 HDD Exit Pit Dredging

A single-point scenario was modelled for the excavation of the HDD exit pit. The following construction characteristics were assumed:

- Excavation method: suction dredging;
- Location: Kilometer Point (KP) 1.5 of the export cable route, Easting 367220 m, Northing 4599161 m in the NAD83/UTM Zone 19N coordinates system, reference water depth is 8 m MLLW;
- Duration: 0.5 day, continuous (no interruption);
- Type: point source;
- Advance rate: N/A;
- Production rate: 90 cubic meters per hour (m^3/hr) (396 gallons per minute [gpm]);
- Released Amount: 100 percent; and
- Release height centered 1.5 m (4.9 ft) above local seabed.

The metocean conditions for the 0.5-day duration represented Spring and Neap Tides selected from the winter and spring seasons. This combination attempts to represent the greatest range of metocean conditions expected during the construction activity (see Section 2.4).

The total number of simulations was two: one Spring Tide simulation and one Neap Tide simulation.

2.2 Export Cable Corridor

Mayflower Wind is considering three offshore export cable corridor options through the Muskeget Channel, namely the Western, the Central, and the Eastern Options. The length of

the offshore export cable corridor from the Lease Area to the landing location is up to 140 km (87 miles [mi]).

Due to the significant overlap between the three corridor options, it was decided with Mayflower Wind to model the Central Option only (total length equal to 88 km [55 mi]), as it is considered to be representative of the other corridor options. To account for the heterogeneity, the offshore export cable corridor, with the Central Option through Muskeget Channel, was broken into three segments with the following construction characteristics (Figure 2.1):

- Segment 1, KP0 (landfall) to KP20 (20 km [12 mi] length)
  - Excavation method: mechanical plow or jetting;
  - Location: KP0 to KP20 of the cable route, point coordinates and reference water depths presented in Table A.4 (Attachment A);
  - Duration: 4.2 days, continuous (no interruption);
  - Type: line source;
  - Advance rate: 200 m/hr (0.1 miles per hour [mi/hr]);
  - Production rate: 600 m^3/hr (2,642 gpm) based on a dredge trench 3 m deep by 1 m wide;
  - Release amount: 25 percent; and
  - Release height centered 1.5 m (4.9 ft) above local seabed.
- Segment 2, KP20 to KP45 (25-km [16-mi] length)
  - Excavation method: mechanical plow or jetting;
  - Location: KP20 to KP45 of the cable route, point coordinates and reference water depths presented in Table A.5 (Attachment A);
  - Duration: 5.2 days, continuous (no interruption);
  - Type: line source;
  - Advance rate: 200 m/hr (0.1 mi/hr);
  - Production rate: 800 m^3/hr (3,522 gpm) based on a dredge trench 4 m deep by 1 m wide. This production rate is 200 m^3/hr (881 gpm) larger than for Segments 1 and 2, in order to accommodate for the effect of potential pre-sweeping of sand waves via suction dredging;
  - Release amount: 25 percent; and
  - Release height centered 1.5 m (4.9 ft) above local seabed.
- Segment 3, KP45 to KP88 (43 km [27 mi] length)
  - Excavation method: mechanical plow or jetting;
  - Location: KP45 to KP88 of the cable route, point coordinates and reference water depths presented in Table A.6 (Attachment A);
  - Duration: 9.0 days, continuous (no interruption);
  - Type: line source;
  - Advance rate: 200 m/hr (0.1 mi/hr);
  - Production rate: 600 m^3/hr (2,642 gpm) based on a dredge trench 3 m deep by 1 m wide;

- Release amount: 25 percent; and
- Release height centered 1.5 m (4.9 ft) above local seabed.

Advance rates, release amounts and heights are typical of cable installation tooling and vessels employed using the associated methods. Jetting typically releases more turbidity than other installation methods and is herein considered as the worst-case installation method for the purpose of scenarios definition. Production rates are computed based on the advance rates and typical trench dimensions. For Segment 2, an increase of production rate of 200 m^3/hr (881 gpm) is considered in order to include potential pre-sweeping of sand waves.

The total duration of the excavation through the export cable route is modelled as 18.2 days. Excavation is assumed to take place in the KP direction, going from KP0 (landfall) to KP88. This is a representative installation scenario – magnitude of impacts will be similar if the excavation were to occur in the opposite direction (KP88 to KP0).

Metocean conditions were extracted for an 18.2-day period in the summer season. That period is inclusive of Spring and Neap Tide conditions. The specific 18.2-day period was determined based on the severity of metocean conditions during the spring and summer seasons. It was chosen to be representative of the variability of the metocean condition during which the construction activity could take place (see Section 2.4).

2.3 Inter-array Cables

A representative inter-array cable route crossing the Lease Area was selected to represent the scenario of inter-array cabling excavation (Figure 2.1). It is considered to be representative of the range of water depths and locations within the Lease Area. The following construction characteristics were assumed:

- Excavation method: Mechanical Cutting ROV/Jetting ROV;
- Location: point coordinates and reference water depths presented in Table A.7 (Attachment A);
- Duration: 9.2 days, continuous (no interruption);
- Type: line source;
- Advance rate: 200 m/hr (0.1 mi/hr);
- Production rate: 400 m^3/hr (1,761 gpm);
- Released Amount: 25 percent; and
- Release height: 1.5 m (4.9 ft) above local seabed

Advance rates, release amounts and heights are typical of cable installation tooling and vessels employed using the associated methods. Jetting typically releases more turbidity than other installation methods and is herein considered as the worst-case installation method for the purpose of scenarios definition.

Metocean conditions for the 9.2-day period, represented the summer season which is the anticipated period for installation. That period is inclusive of Spring and Neap Tide conditions. The specific 9.2-day period was determined based on the severity of metocean

conditions during the summer season. It was chosen to be representative of the variability of the metocean condition during which the construction activity could take place (Section 2.4).

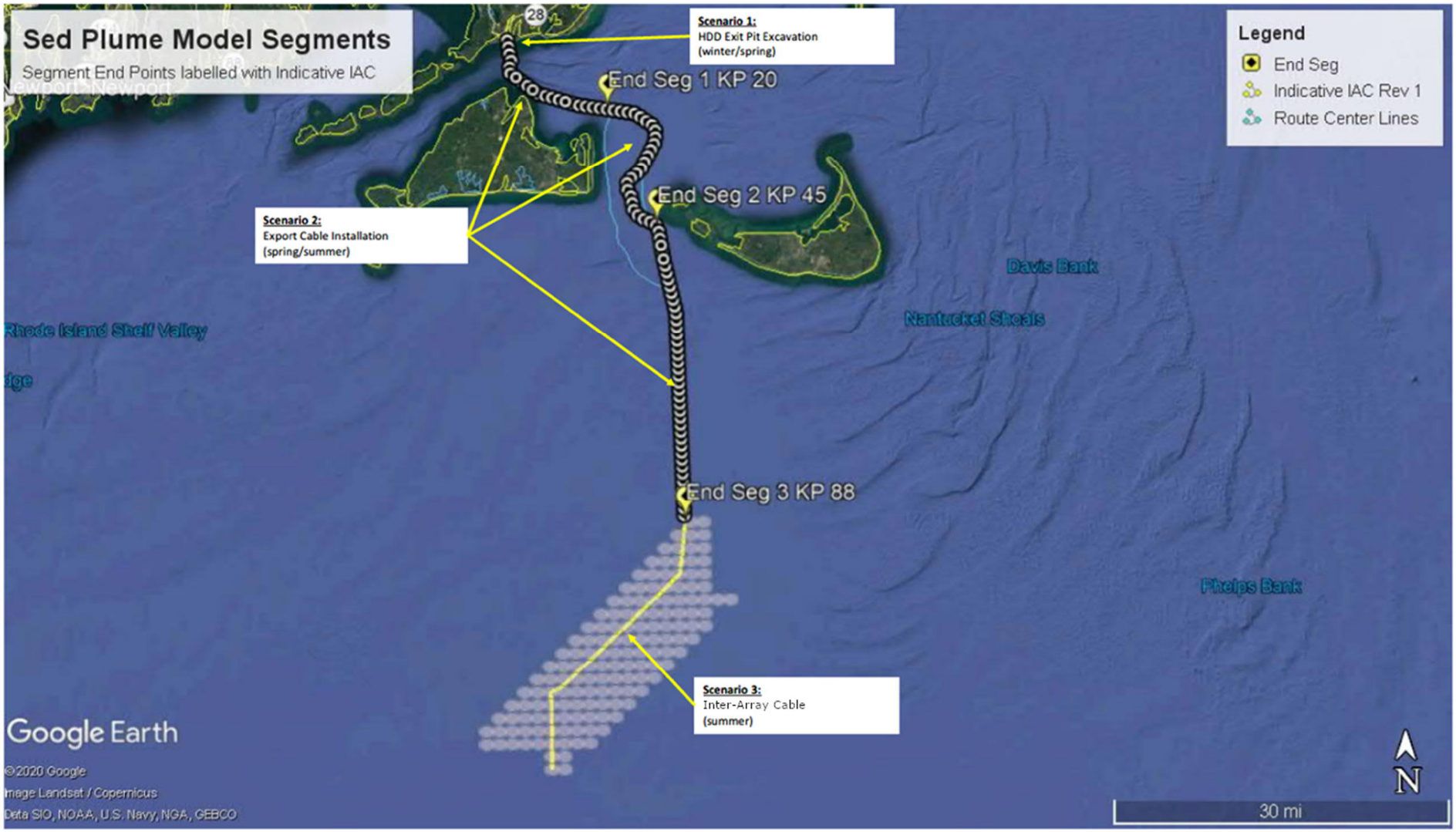

Figure 2.1: Summary of the construction modelling scenarios.

2.4 Input Geotechnical, Bathymetric and Metocean data

The construction scenarios make use of a variety of input data including:

- Grain size distribution (or Particle Size Distribution, PSD) data from grab samples collected during two benthic survey campaigns (May 2020 and August 2020) in the Lease Area and offshore export cable corridor;
- Bathymetric data from site-specific surveys and publicly available sources (see Attachment A for details);
- Coordinates of the HDD exit pit (based on preliminary estimate of location), of the offshore export cable corridor (Central Option) and of the representative inter-array cables.

Metocean conditions, which are a key driver to the sediment plume dispersion assessment, were obtained from the high-resolution metocean model specifically developed for this Project (Section 3 and Attachment B); Details are provided in Attachment A.

Sediment grain size distributions were based on surficial sediment information from the two abovementioned benthic survey campaigns. Each construction scenario will consider a specific PSD table, representative of the sediment within each of the locations. Each modelling segment of the export cable route will use a single, representative PSD table. The release will contain the same PSD as surficial sediment. Table 2.1 shows the assumed PSDs for each construction scenario.

Table 2.1: Input Particle Size Distributions for the modelling of each construction scenario.

Particle type	Median particle diameter [µm]	Particles distribution: ratio for each particle [%]				
		HDD exit pit	Seg 1, Offshore Export Cable Corridor	Seg 2, Offshore Export Cable Corridor	Seg 3, Offshore Export Cable Corridor	Inter-array Cables
Boulder	512,000	0.1	0.1	0.1	0.1	0.1
Cobbles	160,000	0.1	0.01	0.01	0.1	0.1
Pebble	34,000	0.6	6.6	17.7	0.2	0.2
Granule	3,000	1.2	2.3	3.5	0.8	1.0
Very Coarse Sand	1,500	12.0	11.8	7.0	6.4	2.6
Coarse Sand	750	59.5	40.0	25.8	27.0	4.3
Medium Sand	375	24.8	26.0	23.2	29.7	8.1
Fine Sand	187.5	0.8	7.3	16.6	15.8	17.0
Very Fine Sand	93.75	0.2	2.3	3.3	14.6	43.8
Silt	32.225	0.4	3.2	2.4	4.4	19.4
Clay	1.465	0.1	0.5	0.4	0.9	3.5

The metocean conditions, selected for the modelling of each construction scenario represent time series of current speed and direction throughout the water column. The time series of

currents vary spatially along the offshore export cable corridor and along the representative inter-array cables. The time series also vary according to where the sediment plume is advected. Figure 2.2 shows example of the seabed and surface current speed conditions at a central location, as well as the sediment release periods associated with each construction scenario.

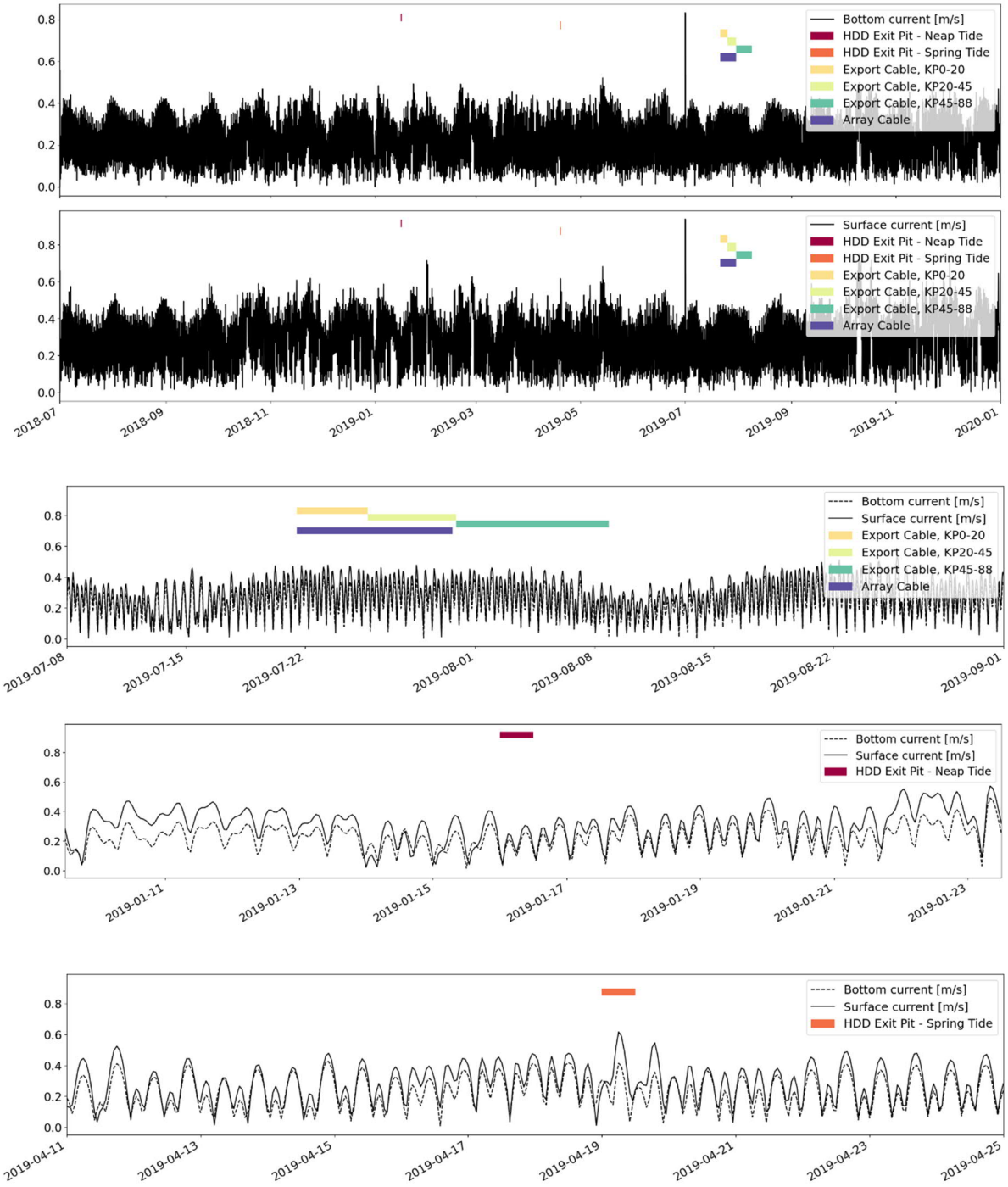

Figure 2.2: Example of input metocean currents used for the modelling of each construction scenario (upper plot), at a central location corresponding to Kilometer Point KP 45 of the offshore export cable corridor (Easting 387315 m / Northing 4573955 m using the NAD 83/UTM Zone 19N) coordinates system. The colored areas represent the sediment release periods associated with each construction scenario. The lower plots show close-up views of both bottom and surface currents focusing on the different sediment release periods. The currents were obtained from the high-resolution metocean model specifically developed for this Project (Section 3 and Attachment B).

3 Metocean Model Development

Site-specific wave and current conditions are needed to correctly assess the dispersion of the sediment plume associated with cable installation activities. In order to fulfil that requirement, a high-resolution wave and current model was developed for the Mayflower Wind Project Area (Lease Area and offshore export cable corridors). Details about the models and formulations are provided in Attachment B.

Here, a brief summary is presented, and focus is given to how the models supported the sediment plume dispersion assessment.

The set of models used is the Coupled Ocean-Atmosphere-Wave-Sediment Transport (COAWST) Modelling System. COAWST is a model coupling toolkit to exchange data fields between the hydrodynamic currents model (ROMS) and the wave model (SWAN).

The SWAN model (Booij et al, 1999) is a third generation shallow-water spectral wave model that includes wave propagation, refraction due to currents and depth, generation by wind, dissipation (white capping, bottom friction, depth-induced breaking), and nonlinear wave-wave interactions. The currents model is the Regional Ocean Modelling System (ROMS), a general class of free surface, terrain-following numerical models that solve the three-dimensional Reynolds-averaged Navier-Stokes equations (RANS) using the hydrostatic and Boussinesq approximations.

The SWAN and ROMS models were used to form a fully two-way coupled modelling system. The coupled system is aimed to better represent the non-linear interactions such as the wave-current interaction, from two independent models.

3.1 Model Set-up

The wave-current grid domain covered the region highlighted in Figure 3.1 which extends from 71.70W to 69.54W and from 40.5N to 41.91N. The domain has a horizontal resolution of about 500 m in the x and y directions. Model bathymetry was built based on the ETOPO1 1-arc minute dataset.

Atmospheric and oceanic boundary conditions were used to downscale the realistic flow and wave fields from global wave-current models to the site-specific wave-current model. Oceanic lateral open boundary conditions and initial conditions for both of the models are as follows:

- Open boundary ocean currents, temperature, salinity and water level were taken from the global HYCOM-NCODA system (www.hycom.org);
- Open boundary tidal constituents were extracted from the Oregon State University TOPEX/Poseidon Global Inverse Solution tidal model (TPXO9.1);

- Open boundary waves were taken from the Fugro Global Wave Database which is an in-house implementation of a WAVEWATCH III model for the global ocean with resolution of 50 km (31 mi).

Both the wave and ocean models employed the same surface boundary condition. Atmospheric forcings were sourced from the American National Centers for Environmental Prediction (NCEP) Climate Forecast System Reanalysis (CFSR).

The models were run for a period of a little over two years (July 1st 2018 to August 31st 2020). Model parameters were outputted at hourly intervals. Standard parameters were outputted (wave and 3d current fields).

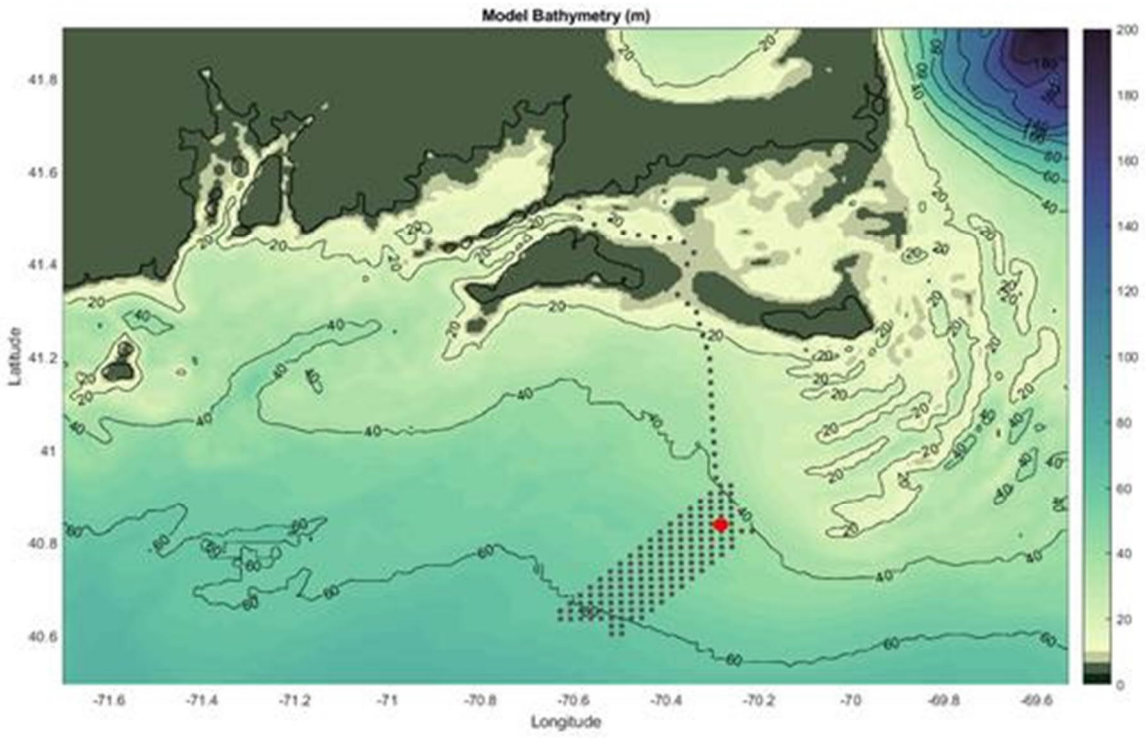

Figure 3.1: Coverage of the wave-current model. Depths are in meters below MLLW. The location of the measurements for validation is represented by a red dot. The Lease Area and the offshore export cable corridor are represented by black dots.

3.2 Model Validation

In-situ metocean measurements were used for model calibration, validation and verification. The measurements were part of the site characterization campaign performed by Fugro in support of the Mayflower Wind Project. A complete description of the measurements, acquisition strategy and quality control are presented in Fugro report no. 143395-0222 00 (Shell USA Mayflower Wind LiDAR Buoy – Service Visit 1 Data Report). A brief description is provided below.

The wind and metocean measurements are from a floating LiDAR buoy deployed just outside the Lease Area at about 43 m (141 ft) of water depth. The approximate coordinates are 40.8413°N, 70.2488°W (Figure 3.1). The buoy system consists of a LiDAR wind sensor, a meteorological mast, a current profiler, a water level sensor and seawater parameter sensors. Fugro deployed the mooring on 23 January 2020. The metocean data used in this study were collected from 23 January to 7 June 2020 during the first service visit (approximately six months).

Data was subject to a detailed quality control procedure. Post-processed, quality-controlled wave and current data were used in this study for model validation and verification.

3.3 Validation of the Wave Model

The wave model has been validated against the data collected in 2020. Figure 3.2 shows the comparison between modelled and observed Significant Wave Height (Hs) together with the wind stress. The correlation between modelled and observed significant wave height is 82 percent. The correlation between Hs and local wind stress is only 50 percent, meaning that some wave energy is generated away from the area and propagates as swell. The correlation coefficients for the period and wave direction are 60 percent and 50 percent, respectively (Figure 3.3 and Figure 3.4).

The Quantile-Quantile (QQ) plot below for the significant wave height show the model tends to overestimate large events (Figure 3.5) when compared to actual data. This is also clear in the time series for some of the events mostly in the period January-February 2020. The overestimation of significant wave height will impact sediment mobility and therefore the results can be seen as conservative in terms of scour potential and plume dispersion.

With respect to wave direction, the model behaves very well for a range of directions (from 50 to 250 degrees). In other words, the model reproduces very well the wave directions coming from NE to SW. For waves from SW to NE the model presents deviations in the direction but for the wave height the accuracy is kept.

Overall, the wave model performance was considered satisfactory and suitable to support the sediment plume dispersion modelling.

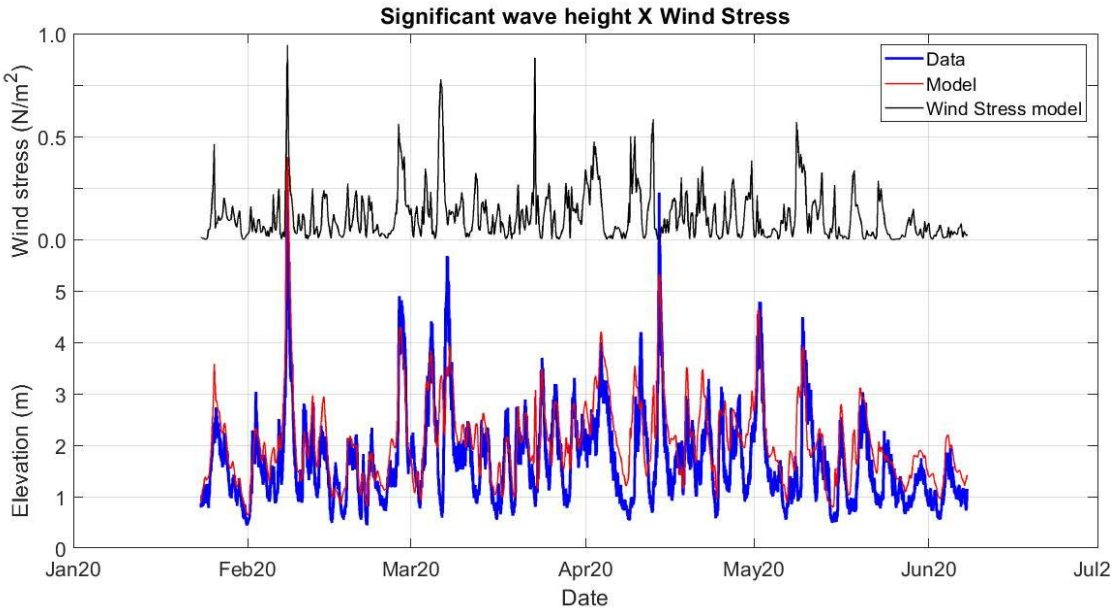

Figure 3.2: Wind stress and significant wave height (Hs). Top panel: wind stress used to drive the model. Bottom panel: Comparison of modelled (red) and observed (blue) Hs.

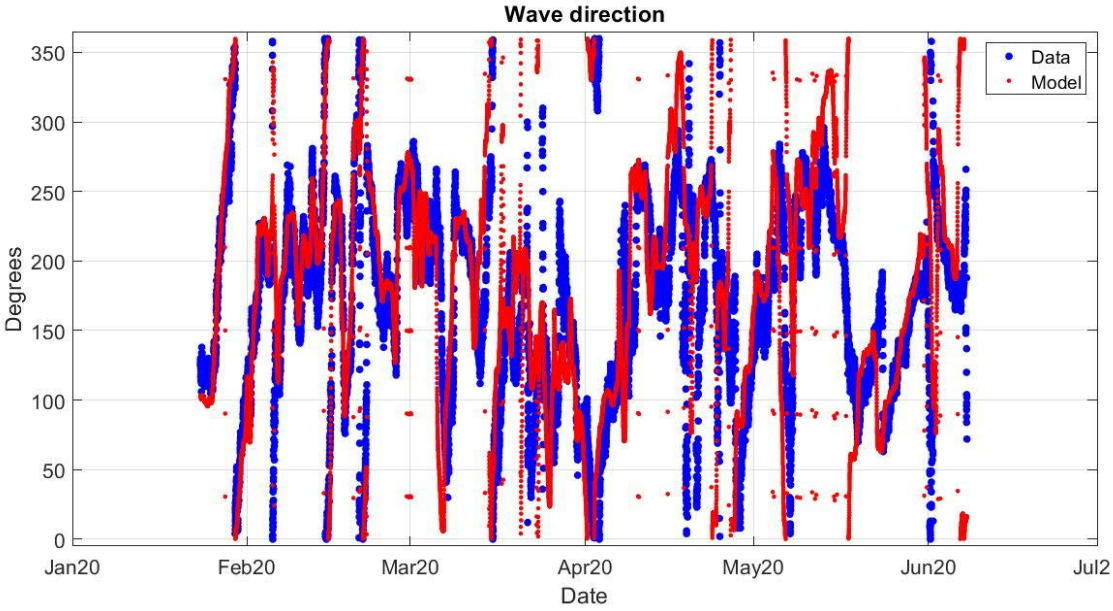

Figure 3.3: Comparison of modelled (red) and observed (blue) wave direction.

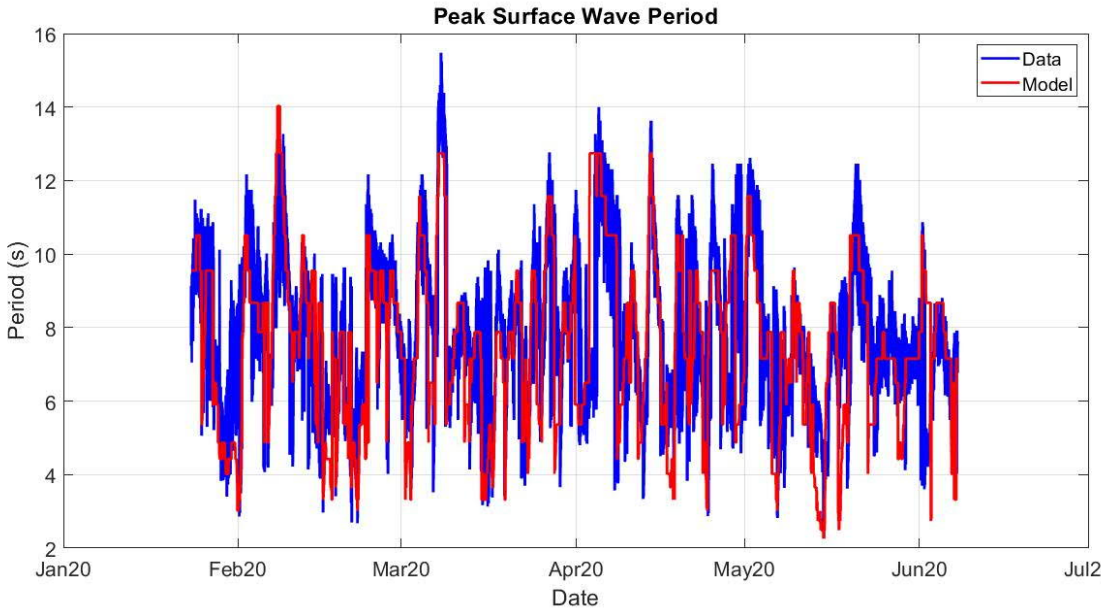

Figure 3.4: Comparison of modelled (red) and observed (blue) peak wave period.

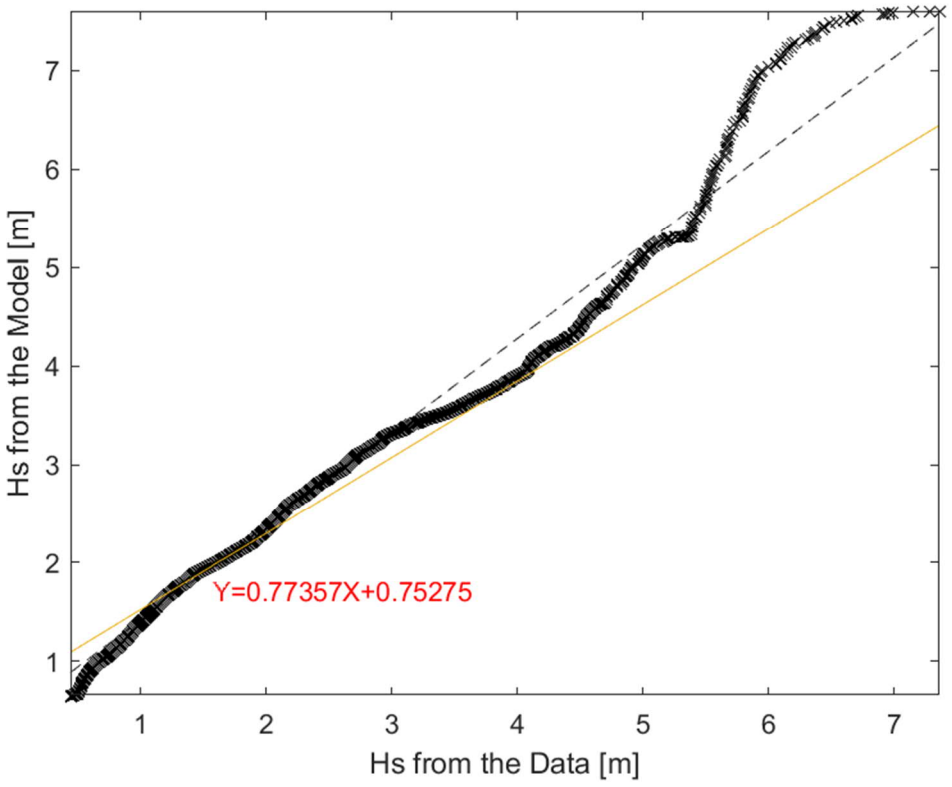

Figure 3.5: Quantile-Quantile plot for the significant wave height. The dashed line represents the slope=1. The yellow line represents the best-fit (y=0.77357x+0.75275).

3.4 Validation of the Ocean Model

Comparison with the in-situ data shows that the ocean model represents current speed statistics very well (Table 3.1), as well as the flux variability frequencies (Figure 3.6 and Figure 3.7). In this comparison, it is possible to notice two main frequencies of variability, one associated with the tide (period of a few hours) and the other associated with the mesoscale currents that flow on the south region of the modelling domain (period of a few days).

Table 3.1: Current speed statistics.

	Mean (m/s)	Standard Deviation	Max (m/s)
Data	0.28	0.12	0.87
Model	0.29	0.15	0.93

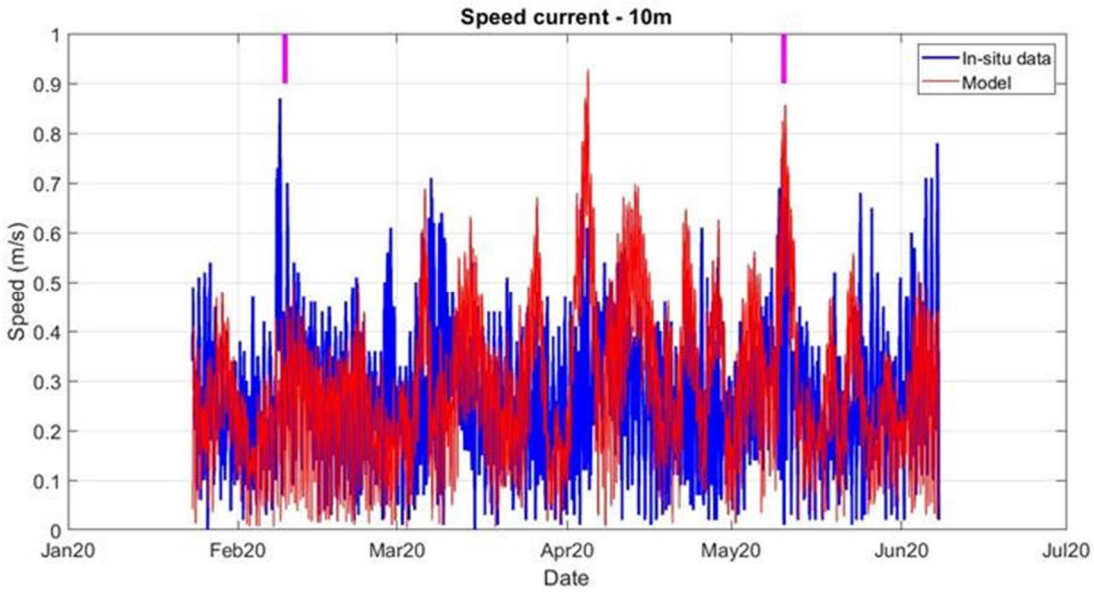

Figure 3.6: Comparison of modelled (red) and observed (blue) 10-m (33-ft) depth speed current.

The main frequencies of variability were separated to identify which signals are important in the study region. For this, a Butterworth filter was used, with a cut-off period of 18 hours, both in the series of observed data and in the model outputs. The comparison of the high frequency series (Figure 3.7) shows that the model is able to represent the variation in intensity of currents associated with the tide well.

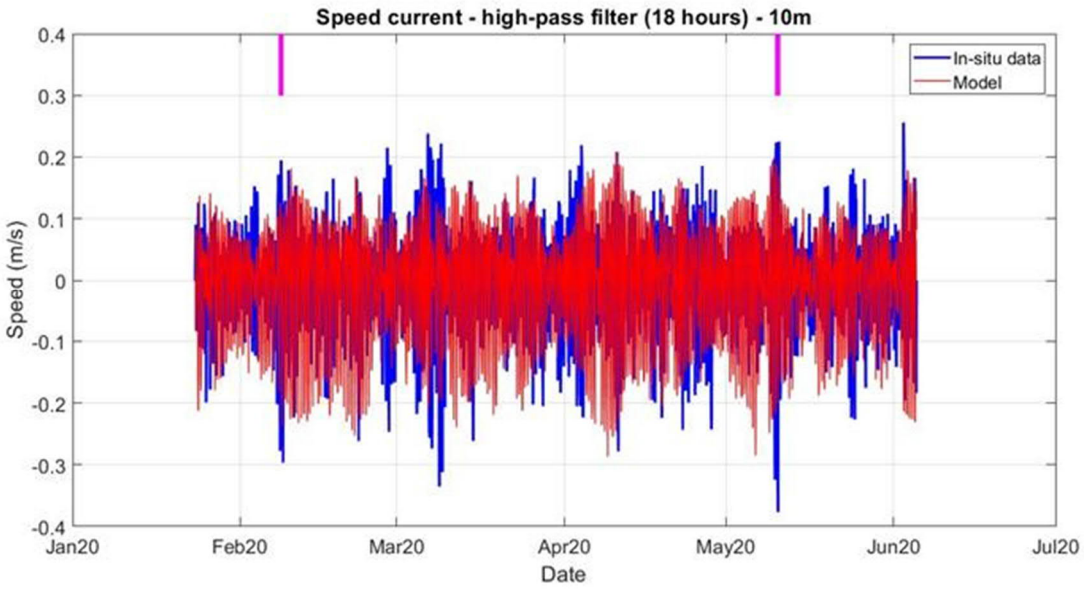

Figure 3.7: Comparison of modelled (red) and observed (blue) high-pass filtered (18 hours) 10-m (33-ft) depth speed current.

Regarding the mesoscale frequency, this will only be well represented if the mesoscale features are present in the global model (HYCOM NCODA), used in the regional model boundaries. As can be seen in Figure 3.6, the ocean model is able to represent the main events well. For a better understanding of these events, the direct comparison at one location must be followed by a spatial analysis.

In the direct comparison (Figure 3.6), both model and data show a strong variation in current intensity, around February 9, 2020 (vertical magenta bar), but the model is unable to capture the intensity peak, present in the data. However, surface current maps show a high intensity westward event present in the global model and being correctly passed through the open boundaries to the regional model (Figure 3.8). It can be noted that there is a more intense flux close to the observation point.

Around May 10, 2020 (vertical magenta bar), when the direct current intensity comparison shows a strong correlation between data and model (Figure 3.6), it is possible to notice an eastward high energy event in both models (Figure 3.9).

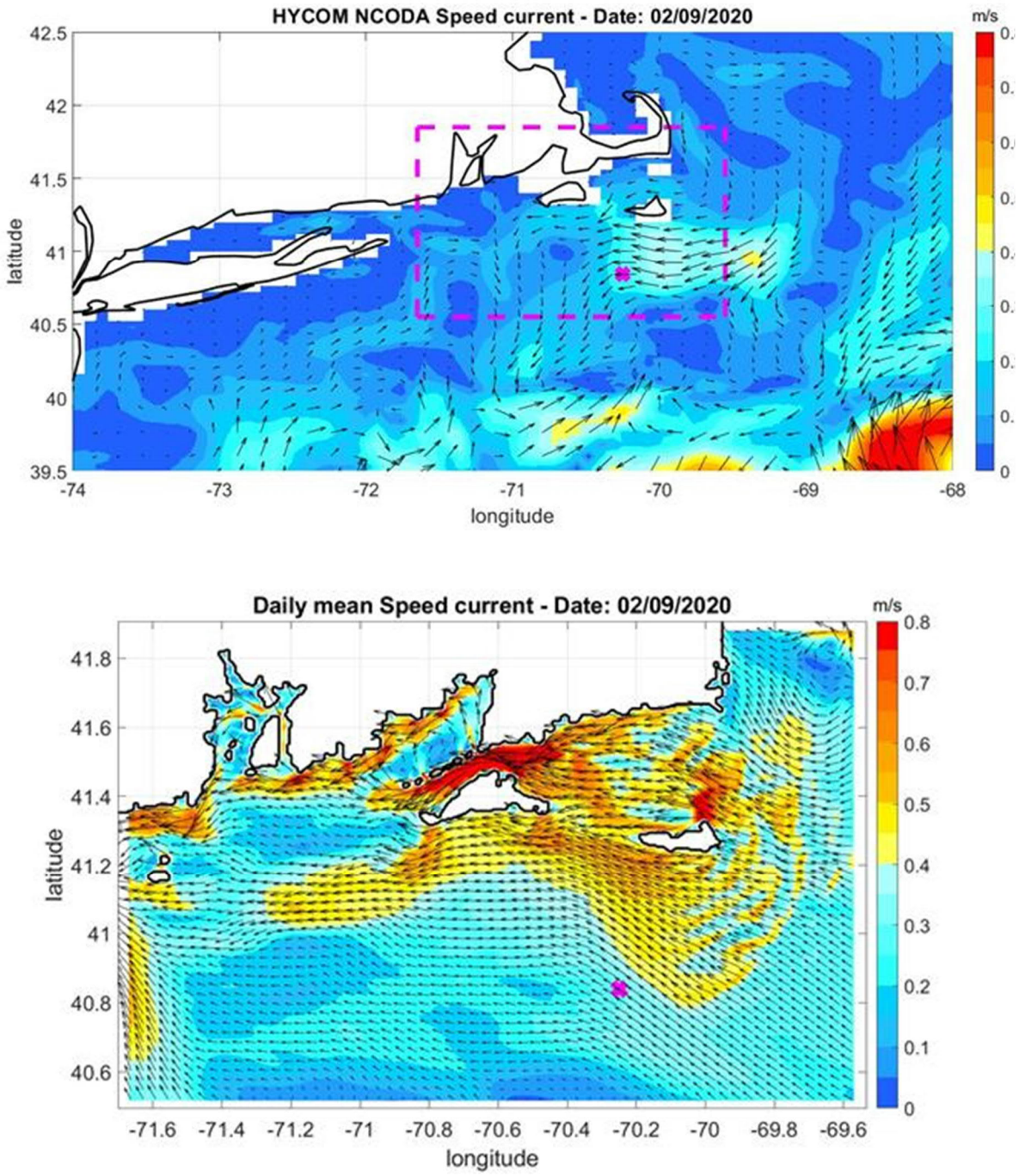

Figure 3.8: Surface currents maps on Feb 9th, 2020. HYCOM NCODA Global model. The ROMS model domain is shown by the magenta box (top); Regional ROMS model (bottom). Observation point marked by a magenta cross.

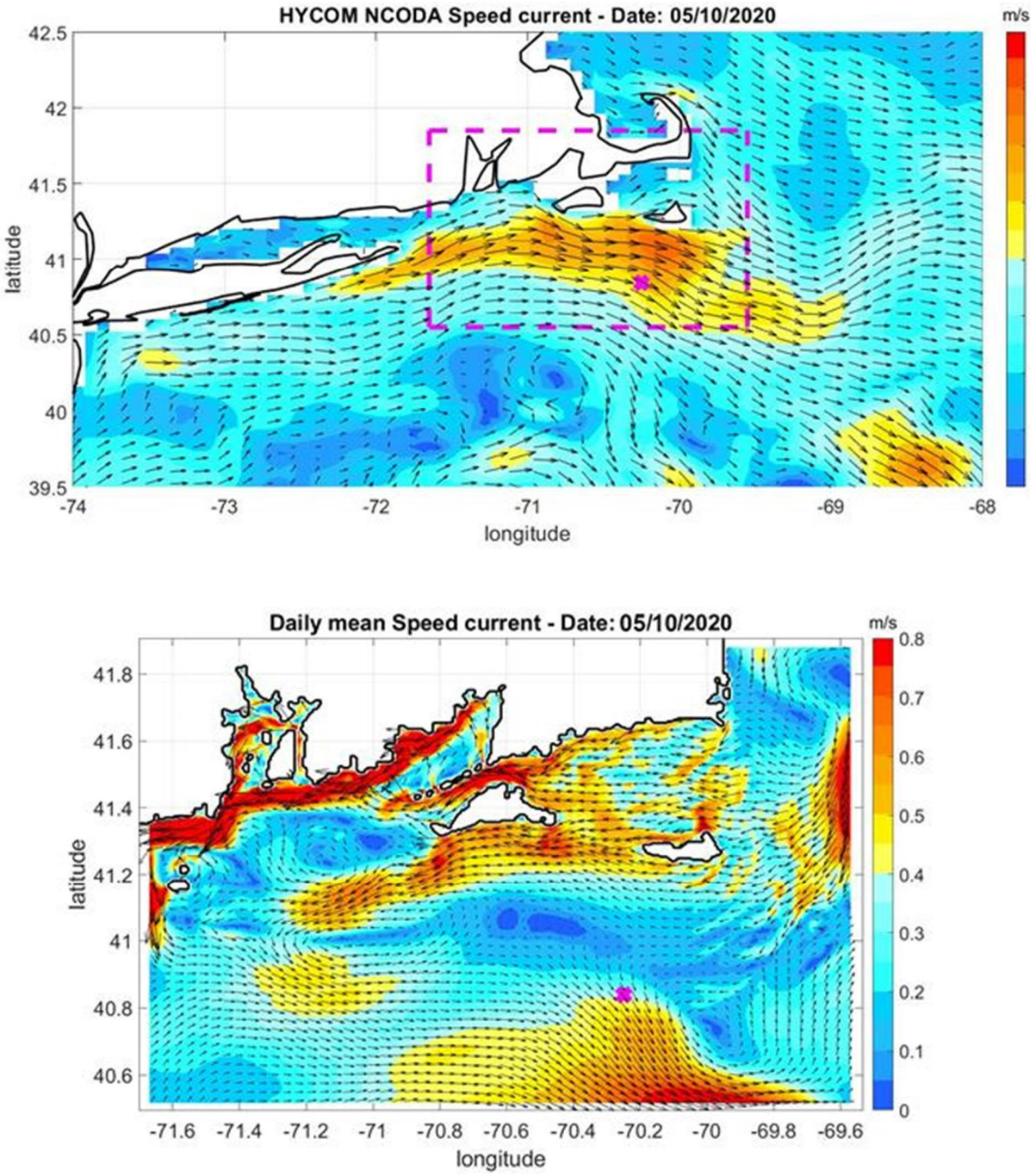

Figure 3.9: Surface currents maps on May 10th, 2020. HYCOM NCODA Global model (top). The ROMS model domain is shown by the magenta box; Regional ROMS model (bottom). Observation point market by a magenta cross.

The comparison between modelled and observed current roses for the low-pass filtered (36 hours) currents shows that the model, at the point of observation, is able to reproduce the frequency of flux intensity and direction very well, this being preferably towards south-southeast (Figure 3.10). In addition, it should be noted that the flow in the region is basically barotropic, that is, there is little vertical variation in intensity and current direction with depth (Figure 3.10).

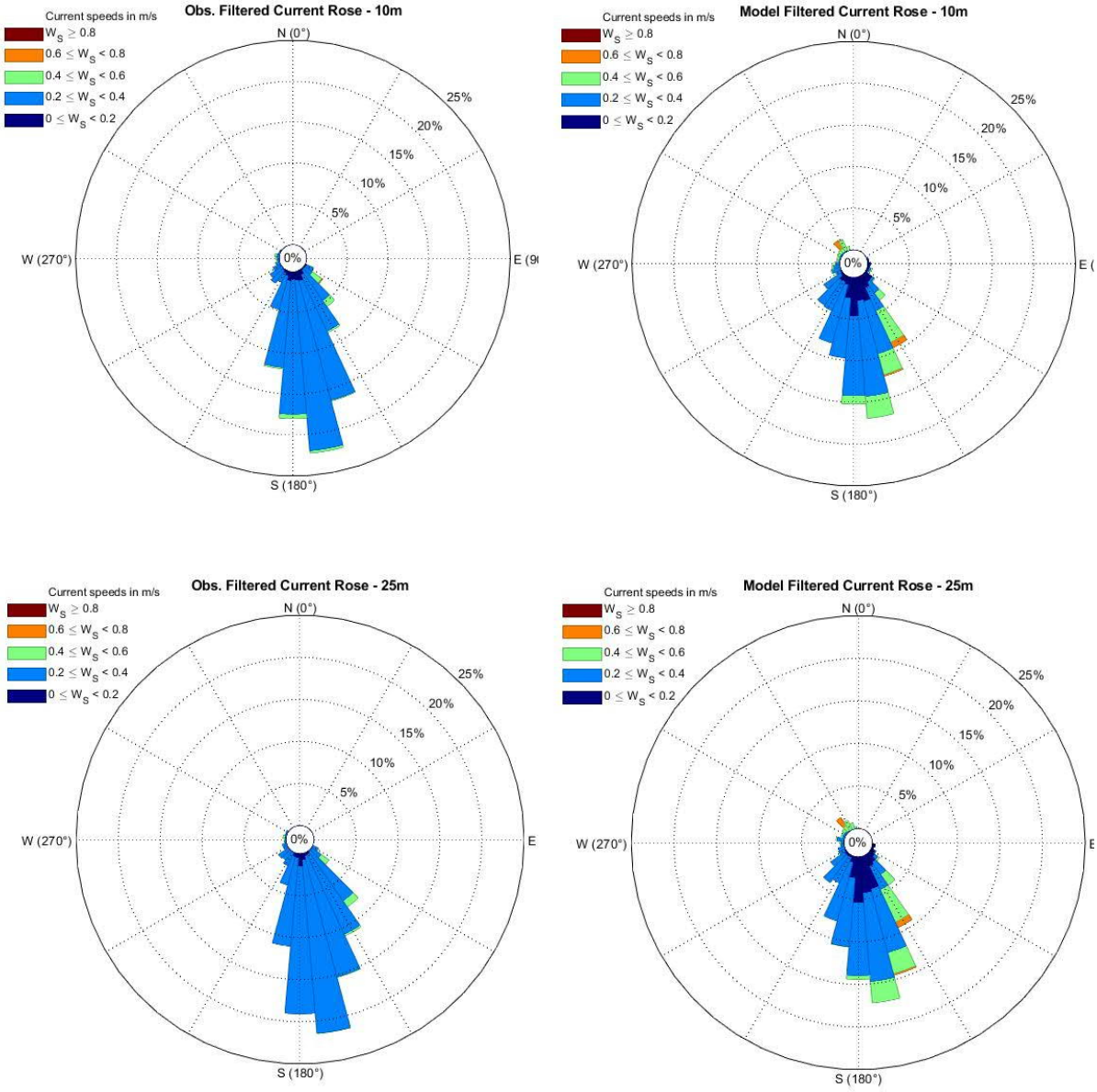

Figure 3.10: Current rose for low-pass current data 10 m (33 ft) below the surface (top left), modelled current data 10 m (33 ft) below the surface (top right),current data 25 m (82 ft) below the surface (bottom left), modelled current data 25 m (82 ft) below the surface (bottom right).

In summary, the current model performance was considered satisfactory and suitable to support the sediment plume dispersion modelling.

4 Sediment Plume Dispersion Model

To predict sediment plume dispersion and deposition associated with cable installation, Fugro developed a numerical model capable of simulating sediment dispersion from the release to the moment they reach the seabed. Details about the model formulation are provided in Attachment C. The following provides a brief summary:

The dispersion of the sediment is estimated by releasing lumps of material at regular time intervals and locations, corresponding to the planned activities (trenching/dredging). The amount of sediment material associated with each lump is estimated based on a provided spill rate. Following the best practices, the model considers two consecutive stages:

- Convective descent/ascent in the near-field zone. The discharge consists of a jet of material to simulate the plume trajectory. As the jet descends or ascends, it entrains the ambient fluid and grows in diameter, with its density and velocity approaching those of the ambient fluid. Sediment may settle out and leave the jet plume to continue to the second stage.
- Far-field dispersion and deposition. After they are released from the jet plume, the sedimentary constituents are advected due to the combined effect of the prevailing ambient currents, the fall velocity and the vertical and horizontal diffusion.

The model allows for sediment dispersion studies with a high flexibility, considering the three-dimensional current velocity forcing on variable topography.

The results of the simulations are presented in the form of maps and cross-sections showing the predicted plume extent and characteristics. The model outputs are expressed in terms of TSS in the water column (mg/L) and thickness for sediment deposition (mm). Summary tables are shown, providing the maximum distance and impacted area for selected thresholds of deposits thickness and TSS. Durations for the TSS to drop below selected levels after the end of the release are also provided.

5 Sediment Plume Dispersion: Deposits Impact

This section presents the results associated with the final thickness of deposited sediment resulting from the installation activities for each of the considered modelling scenarios.

5.1 KP0 to KP20 (Segment 1)

Figure 5.1 shows a mapping of the deposition thickness associated with the export cables, Segment 1 (KP0 to KP20). There is an observed corridor with an average width of 21 m (69 ft) centered on the offshore export cable corridor centerline, with deposits exceeding 5 mm (0.2 inches). Thinner deposits are found at larger distances, following a pattern modulated by the tidal signal. These are related with the finest particles whose lower fall velocity results in larger travel distances.

Table 5.1 provides the maximum distance and impacted area for selected thresholds of deposit thickness. Deposits exceeding 1 mm (0.04 inches) are found at maximum 504 m (1,654 ft) from the offshore export cable corridor, with a deposition area of 67 ha (166 acres [ac]).

Table 5.1: Offshore Export Cables, KP0 to KP20. Maximum distance and area of deposition for selected deposition thickness thresholds.

Deposition thickness threshold [mm]	Maximum observed distance from route centreline [m]	Area of deposition exceeding thickness threshold:	
		Total along entire corridor [ha]	Per km of corridor [ha/km]
0.2	953	122	6.1
0.5	698	88	4.4
1	504	67	3.35
5	22	46	2.3
10	17	39	2.0
50	9	9	4.5
100	N/A	0	0

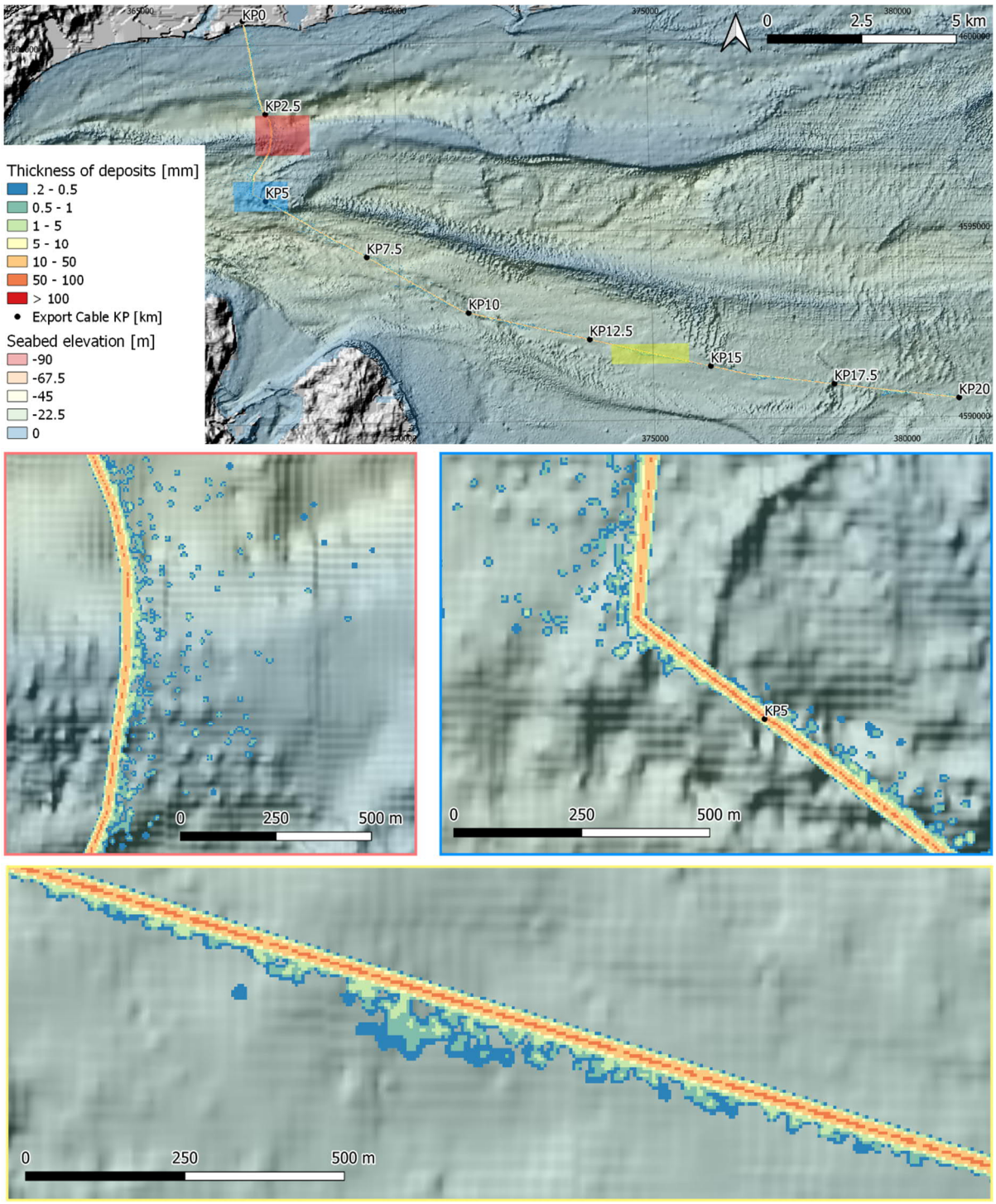

Figure 5.1: Map of deposition thickness associated with the offshore export cable installation, KP 0 to KP 20. The colored rectangular areas indicate the extent of the close-up views framed with corresponding colors.

5.2 KP20 to KP45 (Segment 2)

Figure 5.2 shows a mapping of the deposition thickness associated with the export cable, Segment 2 (KP20 to KP45). There is an observed corridor with an average width of 24 m (79 ft) centered on the offshore export cable corridor centerline, with deposits exceeding 5 mm (0.2 inches). This increased width is related to the increased sediment production rate associated with the pre-sweeping of sand waves. Indeed, for Segment 2, the production rate was increased by an additional 200 m^3/hr (881 gpm), in order to include potential pre-sweeping of sand waves (see Section 2). As discussed in Section 2.2, suction dredging of sand waves was accounted for by an increased trench depth. Similar to Segment 1, deposits of the finest particle sizes are found at larger distances from the cable installation.

Table 5.2 provides the maximum distance and impacted area for selected thresholds of thickness of deposits. Deposits exceeding 1 mm (0.04 inches) are found at maximum 189 m (620 ft) from the offshore export cable corridor, with a deposition area of 97 ha (240 ac).

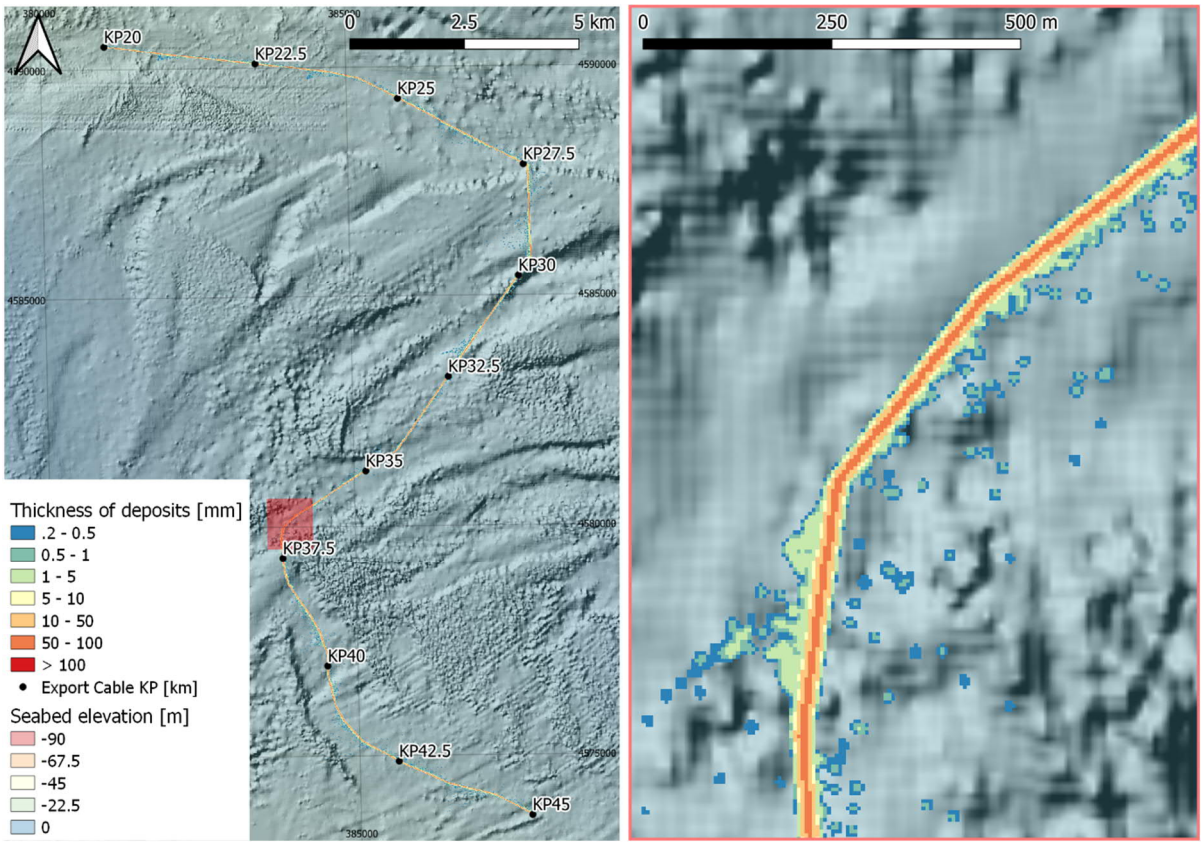

Figure 5.2: Map of deposition thickness associated with the offshore export cable installation, KP 20 to KP 45. The colored rectangular areas indicate the extent of the corresponding close-up view framed with corresponding color.

Table 5.2: Offshore Export Cables, KP20 to KP45. Maximum distance and area of deposition for selected deposition thickness thresholds.

Deposition thickness threshold [mm]	Maximum observed distance from route centreline [m]	Area of deposition exceeding thickness threshold:	
		Total along entire corridor [ha]	Per km of corridor [ha/km]
0.2	721	177	7.1
0.5	438	130	5.2
1	189	97	3.9
5	33	64	2.6
10	27	54	2.2
50	16	22	0.9
100	N/A	0	0

5.3 KP45 to KP88 (Segment 3)

Figure 5.3 shows a mapping of the deposition thickness associated with the offshore export cables, Segment 3 (KP45 to KP88). There is an observed corridor of average width of 20 m (66 ft) centered on the offshore export cable corridor centerline, with deposits exceeding 5 mm (0.2 inches). In comparison with Segments 1 and 2, Segment 3 has a clearly visible tidal influence and a larger amount of sediment deposited in the vicinity of the cable route. Due to the lower currents in this area, a larger amount of sediment is deposited less than 500 m (1,640 ft) away from the cable route, rather than being transported over longer distances.

Table 5.3 provides the maximum distance and impacted area for selected thresholds of thickness of deposits. Deposits exceeding 1 mm (0.04 inches) are found at a maximum 358 m (1,175 ft) from the offshore export cable corridor, with a deposition area of 201 ha (487 ac). The increase of total depositional areas compared with the previous segments must be put in perspective with the increased length of Segment 3 compared to Segment 1 and 2.

Table 5.3: Offshore Export Cables, KP45 to KP88. Maximum distance and area of deposition for selected deposition thickness thresholds.

Deposition thickness threshold [mm]	Maximum observed distance from route centreline [m]	Area of deposition exceeding thickness threshold:	
		Total along entire corridor [ha]	Per km of corridor [ha/km]
0.2	725	347	8.1
0.5	530	253	5.9
1	358	201	4.7
5	88	113	2.6
10	26	86	2.0
50	10	6.8	0.2
100	N/A	0	0

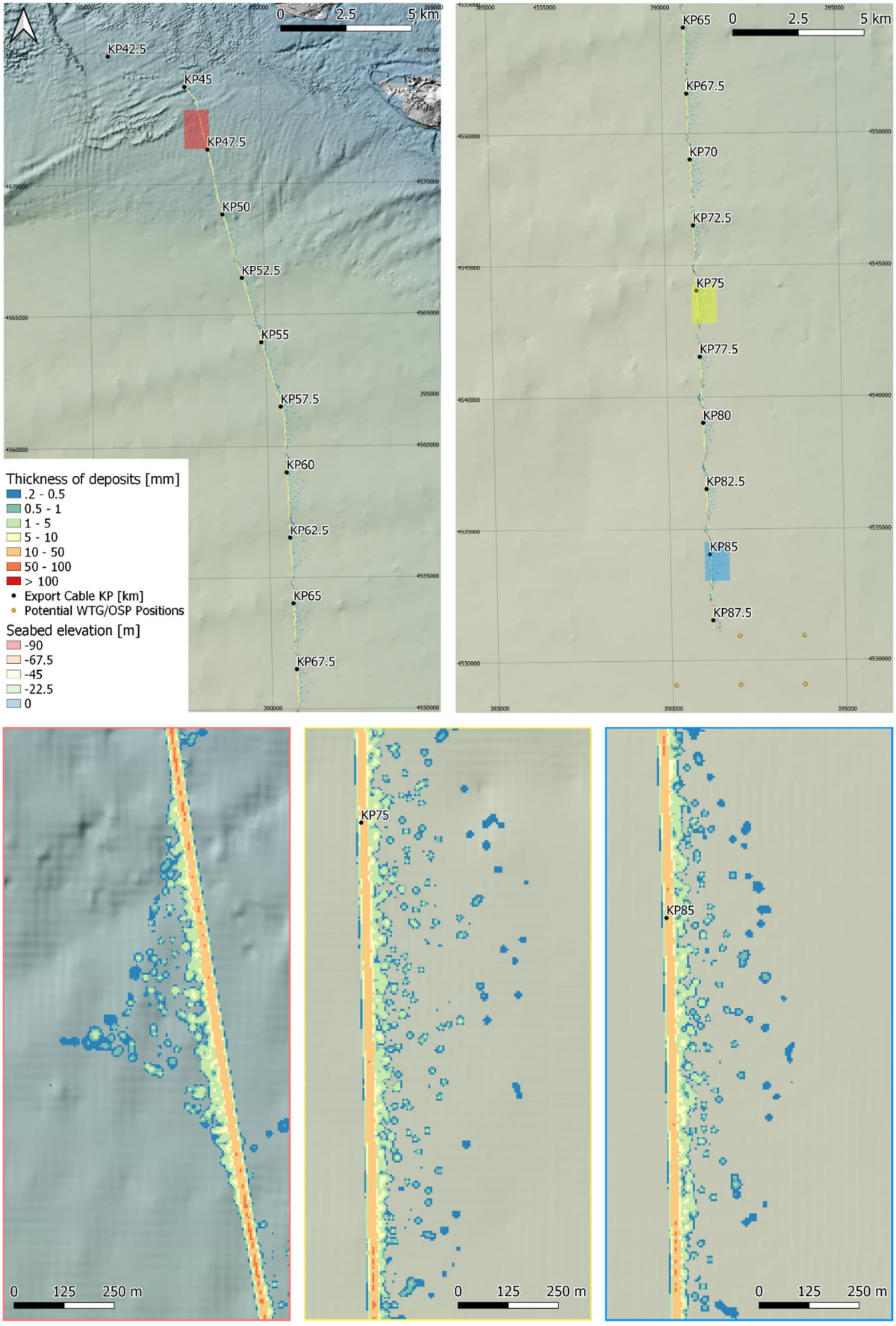

Figure 5.3: Map of deposition thickness associated with the offshore export cable installation, KP 45 to KP 88. The colored rectangular areas indicate the extent of the close-up views framed with corresponding colors.

5.4 Inter-array Cables

Figure 5.4 shows a mapping of the deposition thickness associated with the representative inter-array cables. There is an observed corridor with an average width of 20 m (66 ft) centered on the inter-array cable route, with deposits exceeding 5 mm (0.2 inches). However, deposits in excess of 5 mm (0.2 inches) are also found in several locations outside of this corridor. The low currents characterizing the Lease Area are such that most of the sediment is not transported over long distances but rather deposited within a 1-km (0.6-mi) corridor centered on the inter-array cable route. Further, the PSD in the Lease Area is characterized by a larger amount of fine sediment, susceptible to impact the inter-array cable route, while the larger particles found along the offshore export cable corridor generally settle out very quickly. The tidal influence is clearly visible with a deposition pattern modulated by the tides.

Table 5.4 provides the maximum distance and impacted area for selected thresholds of thickness of deposits. Deposits exceeding 1 mm (0.04 inches) are found at maximum 370 m (1,214 ft) from the inter-array cable route, with a deposition area of 254 ha (628 ac).

Table 5.4: Inter-Array Cables. Maximum distance and area of deposition for selected deposition thickness thresholds.

Deposition thickness threshold [mm]	Maximum observed distance from route centreline [m]	Area of deposition exceeding thickness threshold:	
		Total along entire corridor [ha]	Per km of corridor [ha/km]
0.2	736	538	12.2
0.5	456	345	7.8
1	370	254	5.8
5	180	126	2.9
10	68	76	1.7
50	7	0.02	0.0
100	N/A	0	0

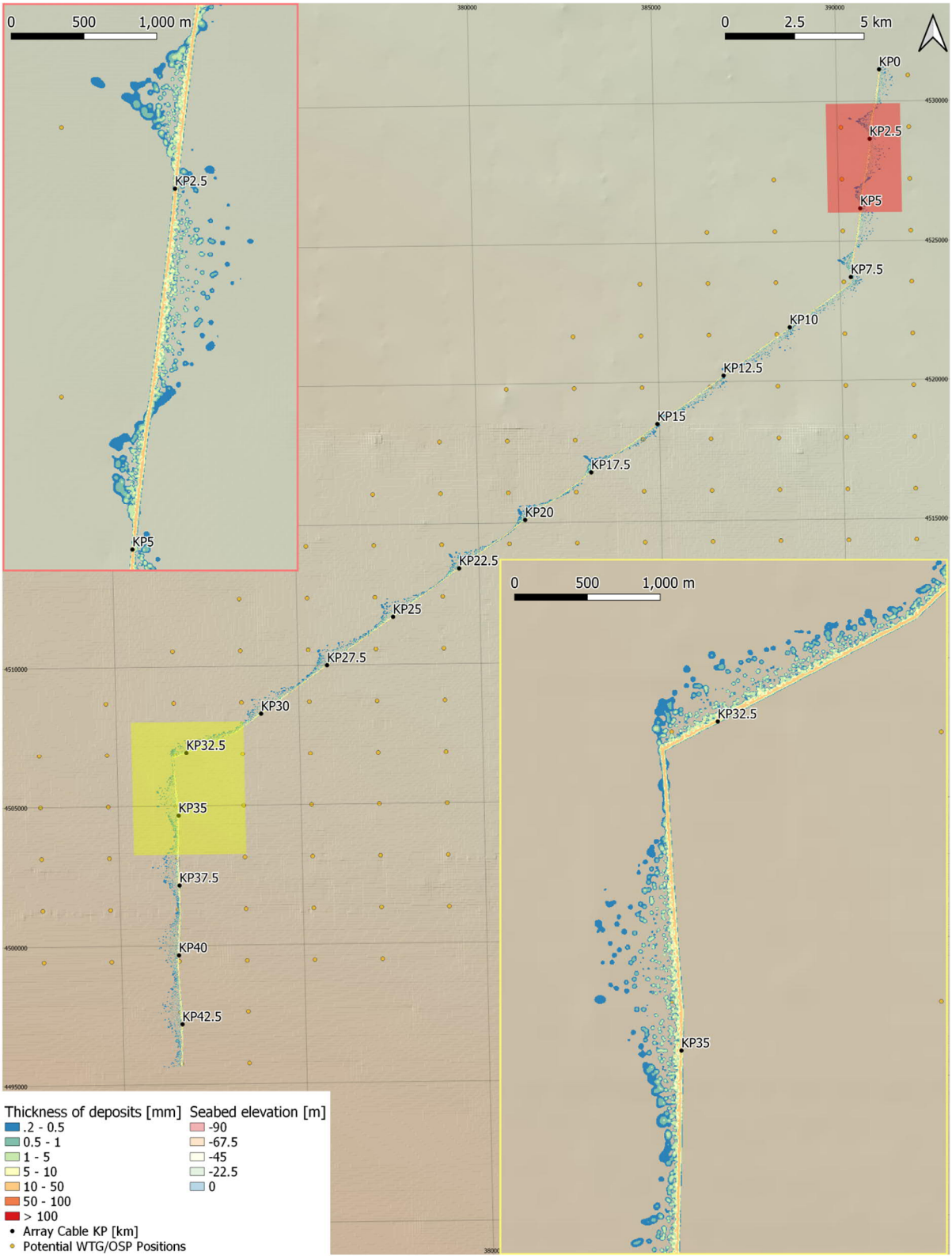

Figure 5.4: Map of deposition thickness associated with the inter-array cable installation. The colored rectangular areas indicate the extent of the close-up views framed with corresponding colors.

5.5 HDD Exit Pit Dredging

The impacted area associated with the HDD exit pit dredging is very limited in terms of deposited sediment (Figure 5.5).

Table 5.5 and Table 5.6 indicate that, for the Neap Tide and Spring Tide scenarios, deposits exceeding 5 mm (0.2 inches) are found at respective maximum distances of 26 m (85 ft) and 32 m (105 ft). For the same thickness of 5 mm (0.2 inches), the impacted area is 0.13 ha (0.32 ac) for both scenarios.

In contrast with the trenching or dredging associated with the installation of cables, the release location for the HDD exit pit does not evolve in time, resulting in more localized deposits. Larger thicknesses of sediment are then observed in the proximity of the release point. As a consequence, while no deposits exceeding 0.1 m (0.3 ft) were observed for the cable installation scenarios, such deposit thicknesses are found for the HDD exit pit, at distances up to 21 m (69 ft) from the release location.

The distribution of deposited sediment is rather similar for both scenarios, although the Neap Tide scenario exhibits deposits on both the western and eastern sides of the release point as the result of tide reversal.

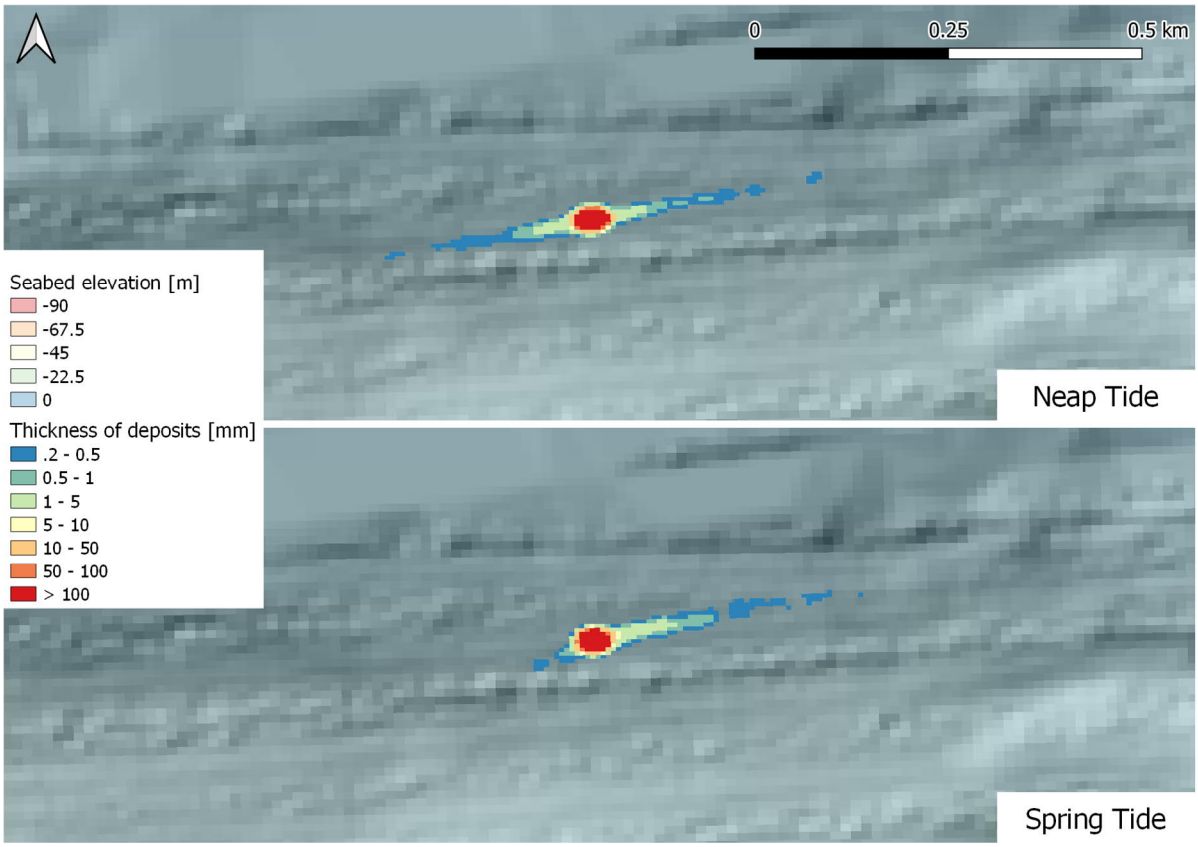

Figure 5.5: Map of deposition thickness associated with HDD exit pit dredging, for Neap (up) and Spring (down) Tide conditions.

Table 5.5: HDD exit pit, Neap Tide. Maximum distance and area of deposition for selected deposition thickness thresholds.

Deposition thickness threshold [mm]	Maximum observed distance from release location [m]	Area of deposition exceeding thickness threshold [ha]
0.2	232	0.69
0.5	123	0.36
1	57	0.24
5	26	0.13
10	26	0.12
50	21	0.09
100	21	0.08

Table 5.6: HDD exit pit, Spring Tide. Maximum distance and area of deposition for selected deposition thickness thresholds.

Deposition thickness threshold [mm]	Maximum observed distance from release location [m]	Area of deposition exceeding thickness threshold [ha]
0.2	271	0.62
0.5	124	0.35
1	88	0.25
5	32	0.13
10	28	0.12
50	24	0.09
100	21	0.07

6 Sediment Plume Dispersion: Maximum TSS Impact

This section presents the TSS resulting from the installation activities for each of the considered modelling scenarios. Maximum TSS values presented on maps are computed based on the maximum values observed during the whole simulation period and along the water column (time- and depth-maximum). Maximum TSS values with vertical structure presented along transects are computed based on the maximum values observed during the whole simulation period (time-maximum).

See Section 7 for discussion of duration of suspended sediment and elevated turbidity.

6.1 KP0 to KP20 (Segment 1)

Figure 6.1 shows a mapping of time- and depth-maximum TSS associated with the installation of the offshore export cables, Segment 1 (KP 0 to KP 20). The turbidity dispersion is mainly governed by longshore currents, with particles mostly travelling along the east-west axis. The presence of tides is responsible for the alternating transport directions observed along the offshore export cable corridor.

Figure 6.2 shows the vertical structure of the maximum TSS observed during the simulation along selected transects visible on Figure 6.1. Observations of sediment concentrations exceeding 50 mg/l (0.00042 pounds per gallon [lb/gal]) are generally limited to the first 5 m (16 ft) from the seabed.

Table 6.1 indicates that sediment concentrations in excess of 10 mg/l (0.00008 lb/gal) are observed at a maximum distance of 1.9 km (1.2 mi) from the offshore export cable corridor and impact an area of 575 ha (1,421 ac). Concentrations exceeding 50 mg/l (0.00042 lb/gal) are observed at a maximum distance of 272 m (892 ft) from the offshore export cable corridor.

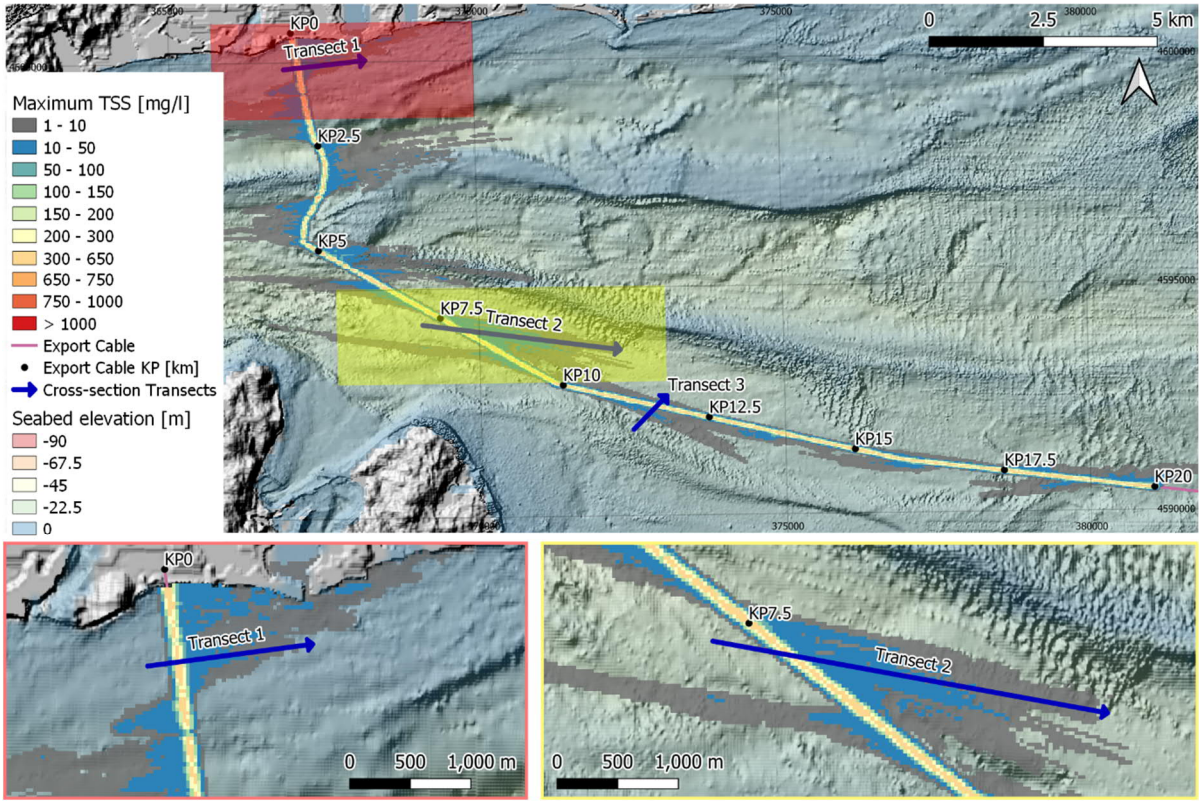

Figure 6.1: Map of maximum sediment concentration associated with the offshore export cable installation, KP 0 to KP 20. The colored rectangular areas indicate the extent of the close-up views framed with corresponding colors.

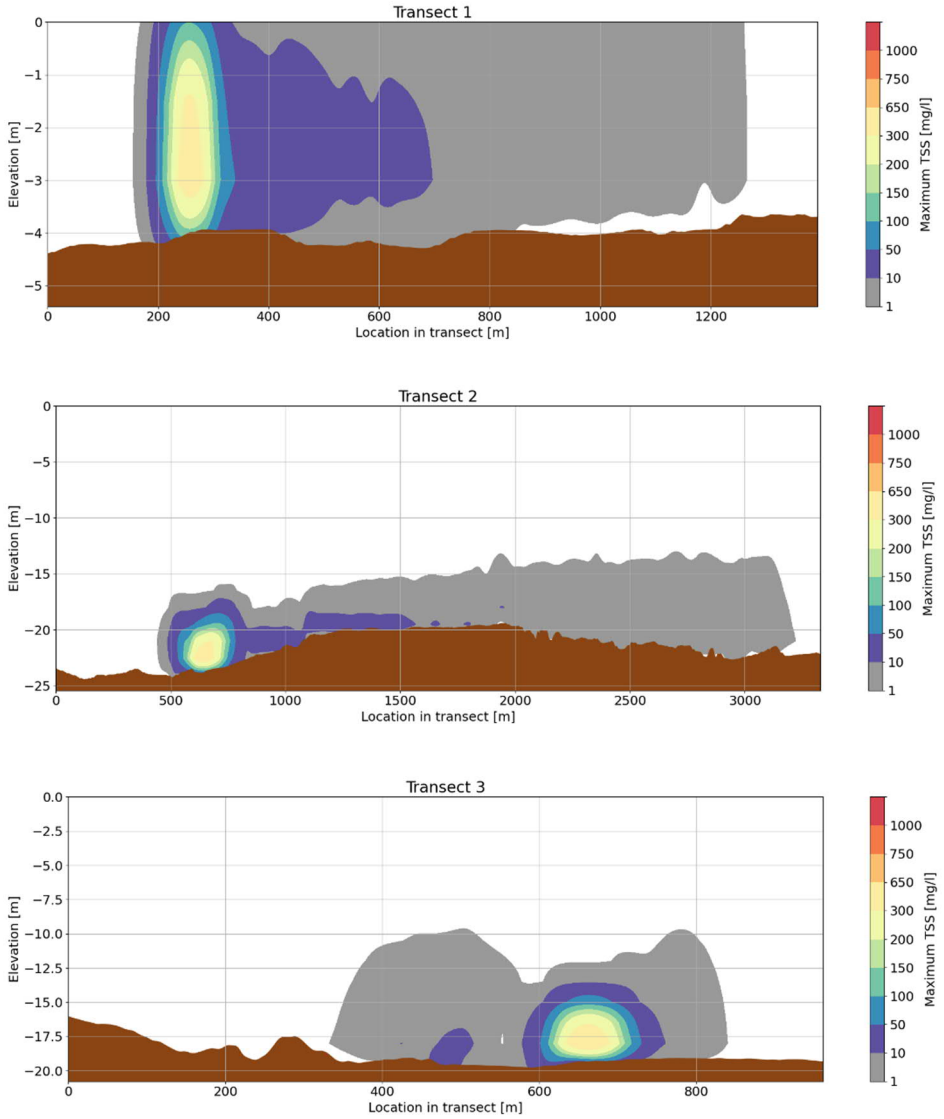

Figure 6.2: Vertical structure along selected transects of maximum sediment concentration associated with the offshore export cable installation, KP 0 to KP 20. The location of the associated transects is depicted in Figure 6.1.

Table 6.1: Offshore Export Cables, KP0 to KP20. Maximum distance and area for selected TSS thresholds.

TSS threshold [mg/l]	Maximum observed distance from route centreline [m]	Area exceeding TSS threshold	
		Total along entire corridor [ha]	Per km of corridor [ha/km]
1	4093	1743	87.2
10	1901	575	28.8
50	272	248	12.4
100	61	196	9.8
150	60	162	8.1
200	51	130	6.5
300	35	79	4.0
650	4	0.2	0.0
750	N/A	0	0
1000	N/A	0	0

6.2 KP20 to KP45 (Segment 2)

Figure 6.3 shows a mapping of time- and depth-maximum TSS associated with the installation of the offshore export cables, Segment 2 (KP 20 to KP 45). From KP 20 to KP 30 particles behave similarly as in the area of Segment 1, travelling mainly along the east-west axis with a TSS pattern modulated by the tides. This alignment evolves for higher KP values within the Muskeget Channel, with particles travelling mostly along the channel axis, following the direction of dominant currents.

Figure 6.4 shows the vertical structure of the maximum TSS observed during the simulation along selected transects visible on Figure 6.3. Observations of sediment concentrations exceeding 50 mg/l (0.00042 lb/gal) are generally limited to the first 5 m (16 ft) from the seabed.

Table 6.2 indicates that sediment concentrations in excess of 10 mg/l (0.00008 lb/gal) are observed at a maximum distance of 2.1 km (1.3 mi) from the offshore export cable corridor and impact an area of 1,105 ha (2,731 ac). Concentrations exceeding 50 mg/l (0.00042 lb/gal) are observed at a maximum distance of 613 m (2,011 ft) from the offshore export cable corridor. These larger travel distances compared with Segment 1 are related to the stronger currents observed in the Muskeget Channel area.

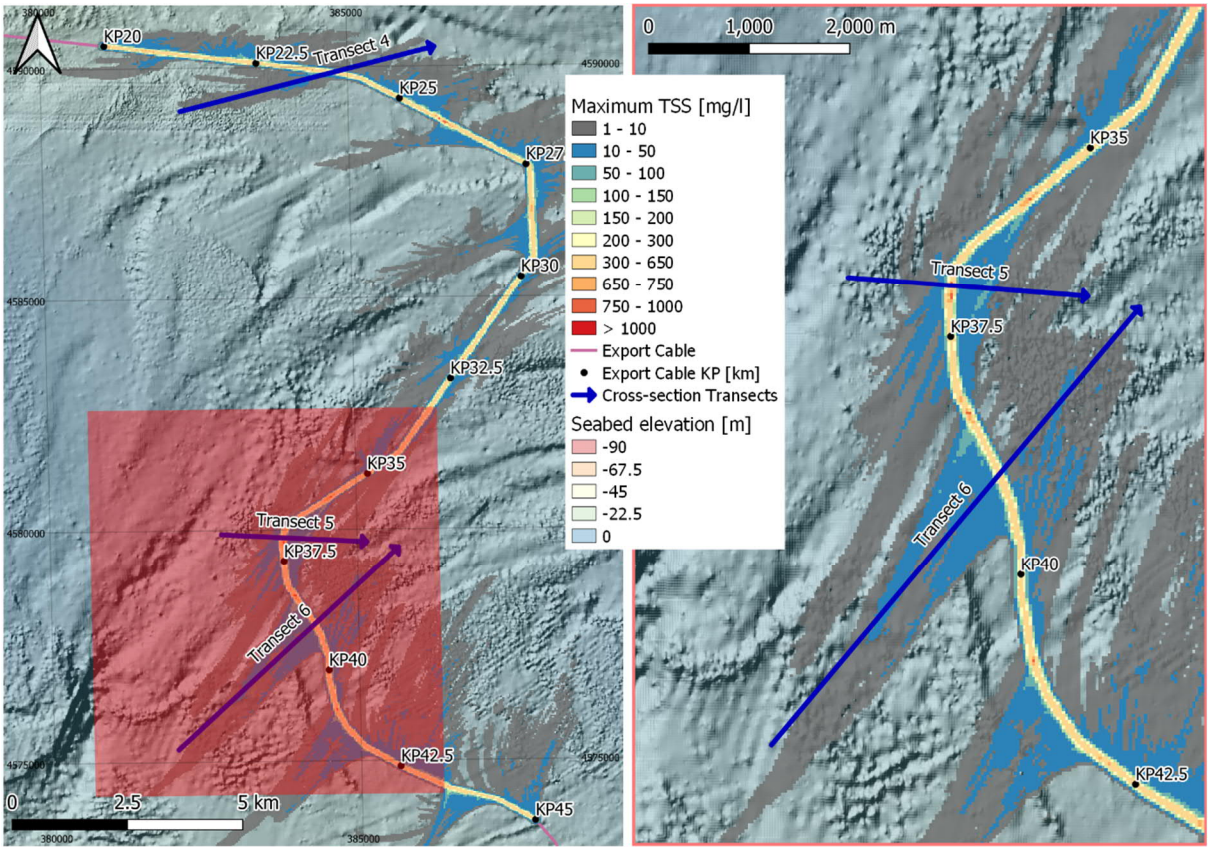

Figure 6.3: Map of maximum sediment concentration associated with the offshore export cable installation, KP 20 to KP 45. The colored rectangular areas indicate the extent of the corresponding close-up view framed with corresponding colors.

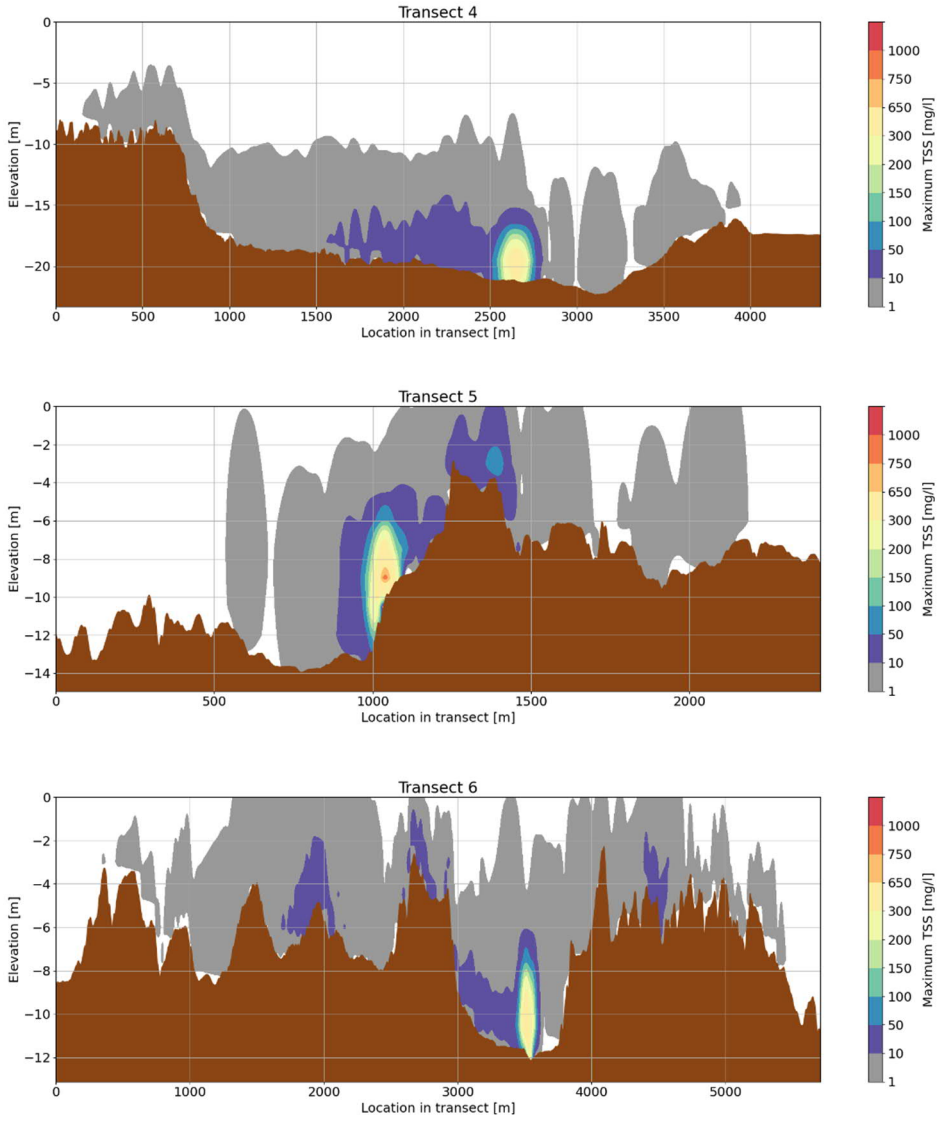

Figure 6.4: Vertical structure along selected transects of maximum sediment concentration associated with the offshore export cable installation, KP 20 to KP 45. The location of the associated transects is depicted in Figure 6.3.

Table 6.2: Offshore Export Cables, KP20 to KP45. Maximum distance and area for selected TSS thresholds.

TSS threshold [mg/l]	Maximum observed distance from route centreline [m]	Area exceeding TSS threshold	
		Total along entire corridor [ha]	Per km of corridor [ha/km]
1	3945	3926	157.0
10	2103	1105	44.2
50	613	362	14.5
100	135	283	11.3
150	68	243	9.7
200	66	213	8.5
300	48	160	6.4
650	26	6.2	0.2
750	22	1.4	0.1
1000	N/A	0	0

6.3 KP45 to KP88 (Segment 3)

Figure 6.5 shows a mapping of time- and depth-maximum TSS associated with the installation of the offshore export cables, Segment 3 (KP 45 to KP 88). Up to KP50, sediment is transported both on the westward and eastward sides of the offshore export cable corridor, while the transport is mostly eastward for larger KPs.

Figure 6.6 shows the vertical structure of the maximum TSS observed during the simulation along selected transects visible on Figure 6.5. Observations of TSS exceeding 50 mg/l (0.00042 lb/gal) are still generally limited to the first 5 m (16 ft) from the seabed.

Table 6.3 indicates that sediment concentrations in excess of 10 mg/l (0.00008 lb/gal) are observed at a maximum distance of 2.8 km (1.7 mi) from the offshore export cable corridor, in the proximity of the Muskeget Channel. South of the Channel, such concentrations are generally found less than 1.2 km (0.75 mi) from the offshore export cable corridor. The associated impact area is 2,180 ha (5,387 ac). Concentrations exceeding 50 mg/l (0.00042 lb/gal) are observed at a maximum distance of 312 m (1,024 ft) from the corridor.

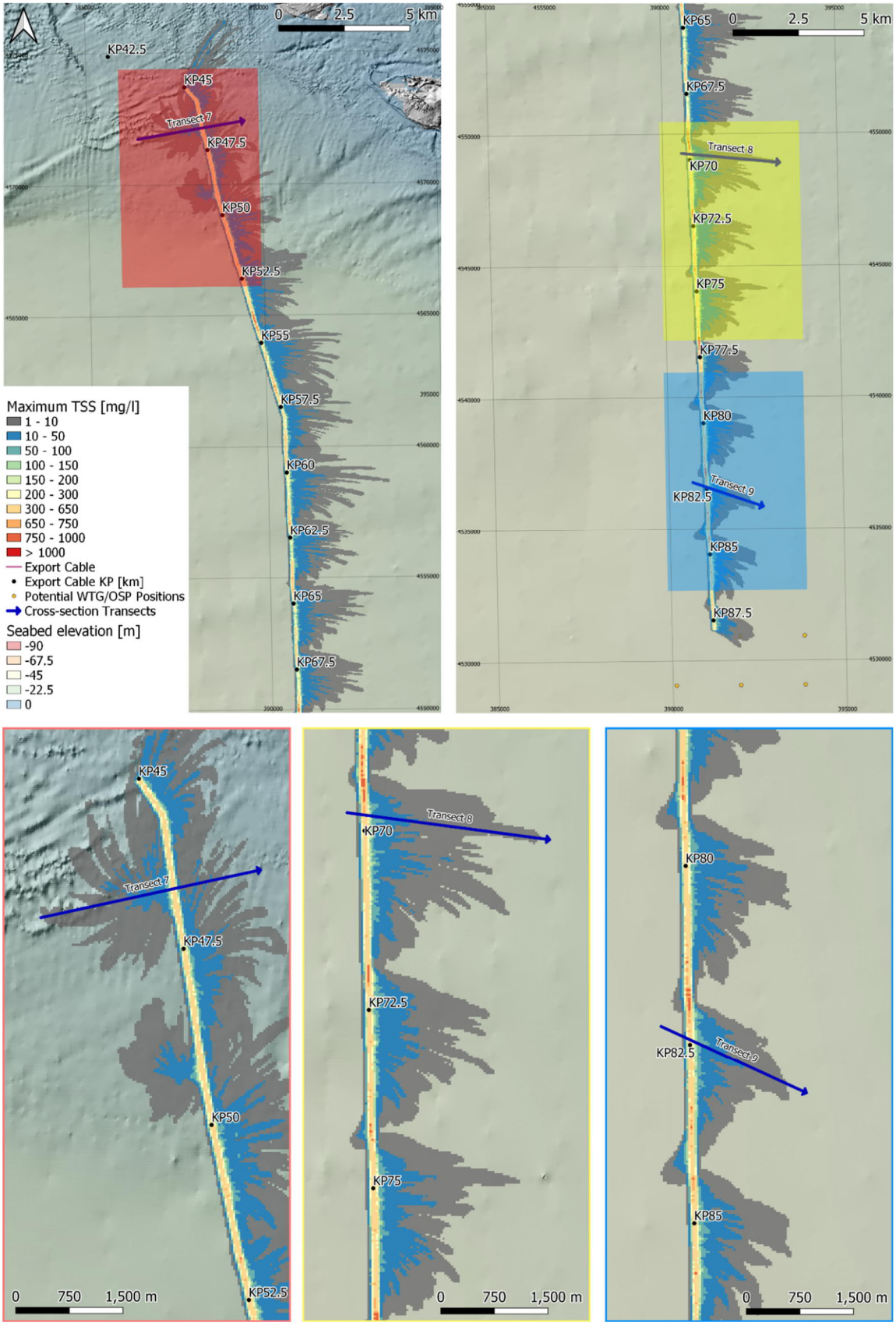

Figure 6.5: Map of maximum sediment concentration associated with the offshore export cable installation, KP 45 to KP 88. The colored rectangular areas indicate the extent of the close-up views framed with corresponding colors.

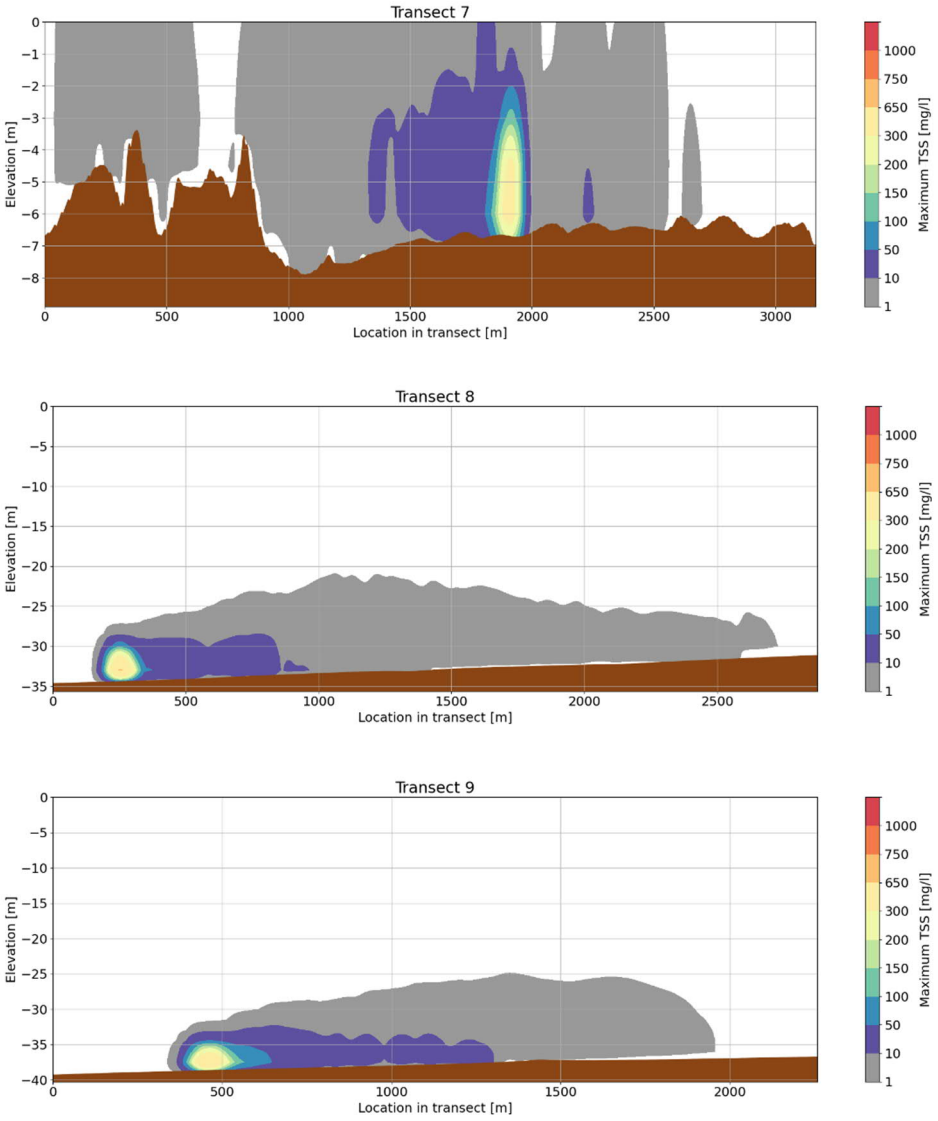

Figure 6.6: Vertical structure along selected transects of maximum sediment concentration associated with the offshore export cable installation, KP 45 to KP 88. The location of the associated transects is depicted in Figure 6.5.

Table 6.3: Offshore Export Cables, KP45 to KP88. Maximum distance and area for selected TSS thresholds.

TSS threshold [mg/l]	Maximum observed distance from route centreline [m]	Area exceeding TSS threshold	
		Total along entire corridor [ha]	Per km of corridor [ha/km]
1	2928	5739	133.5
10	2782	2180	50.7
50	312	750	17.4
100	169	532	12.3
150	93	445	10.3
200	89	373	8.7
300	60	259	6.0
650	26	22	0.5
750	23	8.9	0.2
1000	N/A	0	0

6.4 Inter-array Cables

Figure 6.7 shows a mapping of time- and depth-maximum TSS associated with the installation of the inter-array cables. Up to KP15, sediment is transported both on the westward and eastward sides of the inter-array cable route, while the transport is mostly westward for larger KPs, probably as a consequence of varying currents.

Figure 6.8 shows the vertical structure of the maximum TSS observed during the simulation along selected transects visible on Figure 6.7. Observations of sediment concentrations exceeding 50 mg/l (0.00042 lb/gal) are generally limited to the first 5 to 10 m (16 to 33 ft) from the seabed.

Table 6.4 indicates that sediment concentrations in excess of 10 mg/l (0.00008 lb/gal) are observed at a maximum distance of 1.2 km (0.75 mi) from the inter-array cable route, with an associated impact area of 2,274 ha (5,619 ac). Concentrations exceeding 50 mg/l (0.00042 lb/gal) are observed at a maximum distance of 785 m (2,575 ft) from the route.

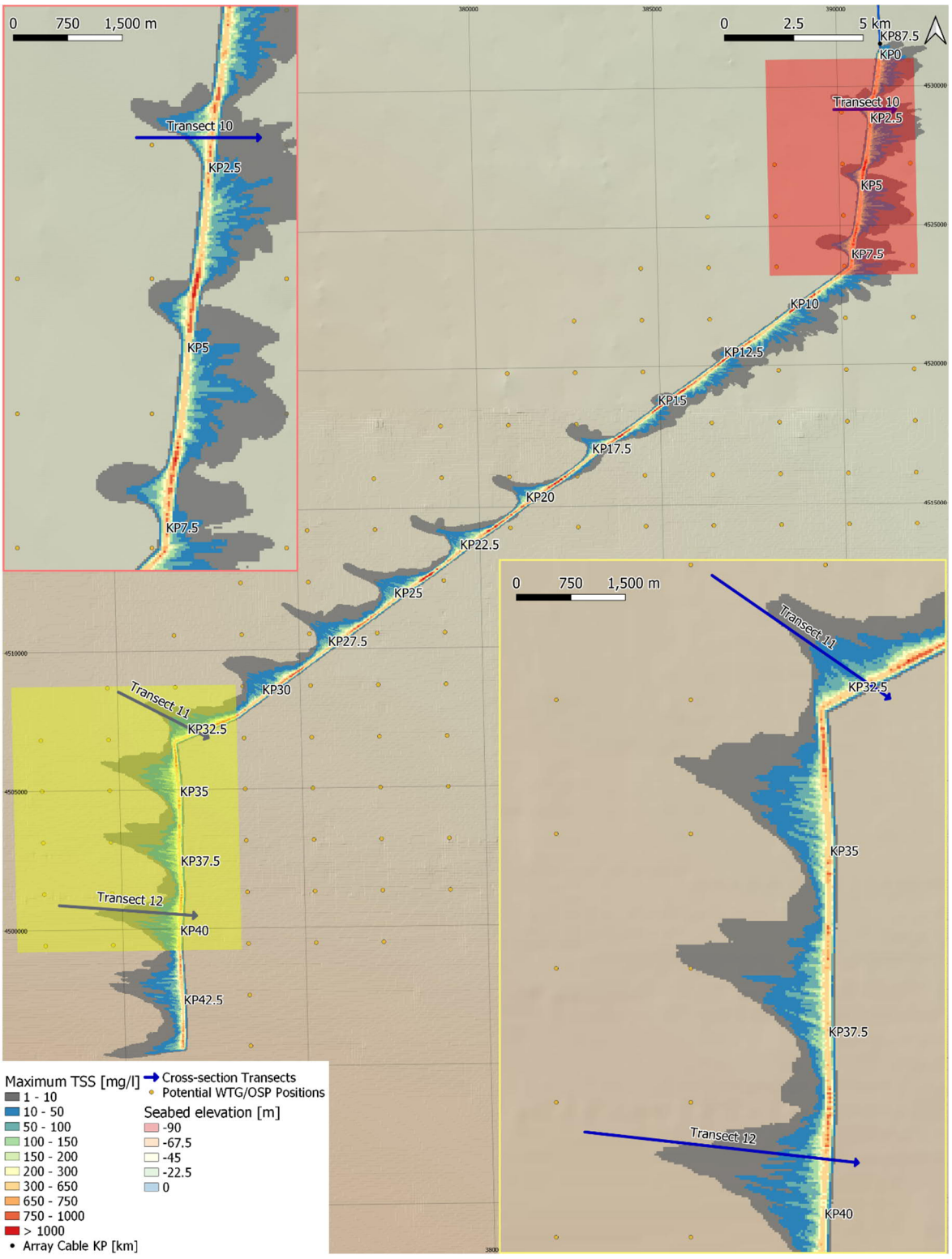

Figure 6.7: Map of maximum sediment concentration associated with the inter-array cable installation. The colored rectangular areas indicate the extent of the close-up views framed with corresponding colors.

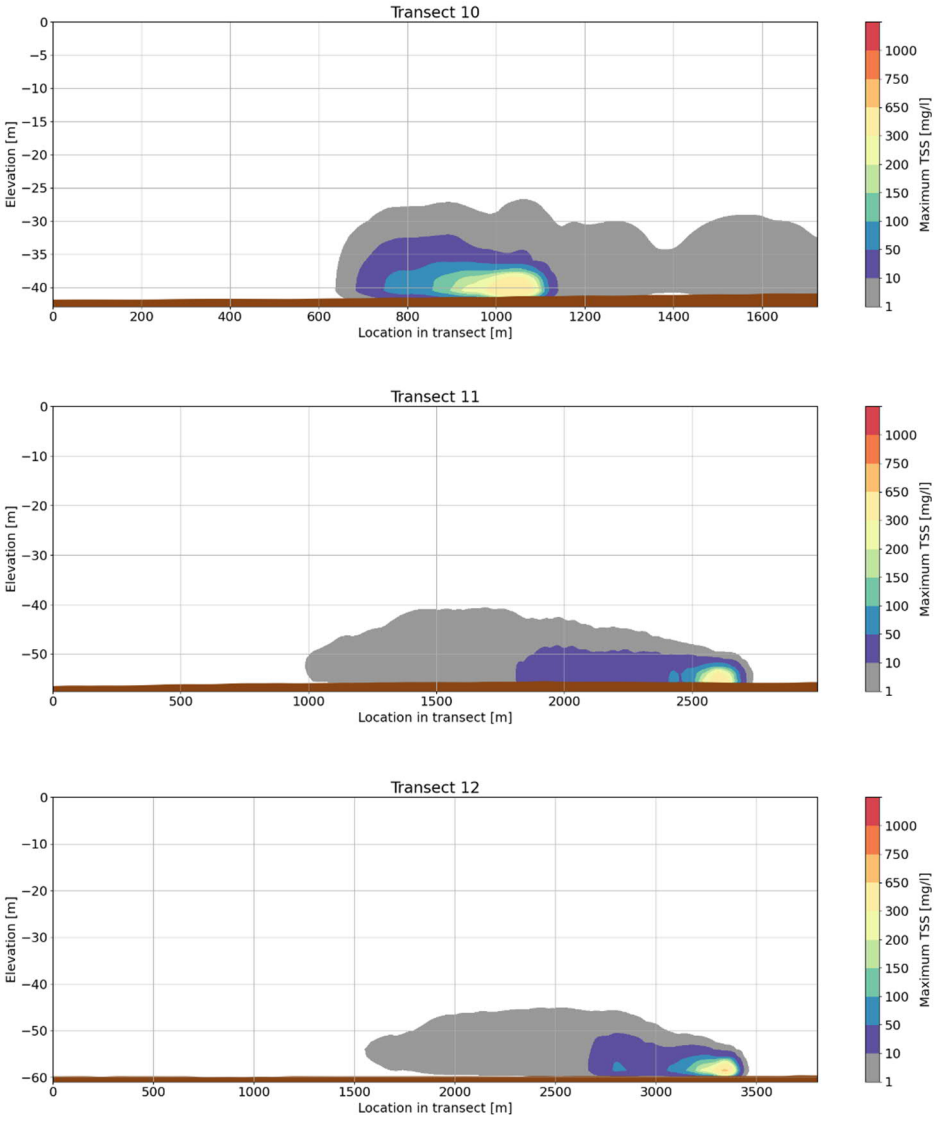

Figure 6.8: Vertical structure along selected transects of maximum sediment concentration associated with the inter-array cable installation. The location of the associated transects is depicted in Figure 6.7.

Table 6.4: Inter-Array Cables. Maximum distance and area for selected TSS thresholds.

TSS threshold [mg/l]	Maximum observed distance from route centreline [m]	Area exceeding TSS threshold	
		Total along entire corridor [ha]	Per km of corridor [ha/km]
1	2366	4580	104.1
10	1243	2274	51.7
50	785	1255	28.5
100	370	838	19.0
150	250	639	14.5
200	190	533	12.1
300	128	397	9.0
650	69	110	2.5
750	49	63	1.4
1000	34	13	0.3

6.5 HDD Exit Pit Dredging

The impacted area associated with the HDD exit pit dredging is rather limited in terms of TSS impact (Figure 6.9, Figure 6.10 and Figure 6.11). Table 6.5 and Table 6.6 indicate that, for the respective Neap Tide and Spring Tide scenarios, sediment concentrations exceeding 10 mg/l (0.00008 lb/gal) are found at a maximum distance of 230 m (755 ft) and 150 m (492 ft). For the same TSS of 10 mg/l (0.00008 lb/gal), the impacted areas are respectively 1.7 ha (4.2 ac) and 1.5 ha (3.7 ac).

As for the deposition, the Neap Tide scenario shows impacted areas in terms of TSS on both the western and eastern sides of the release point as a result of tide reversal. The Spring Tide scenario is associated with significantly larger travel distances and impacted area associated with the finest particles, but this behavior is only visible at very low TSS levels such as 1 mg/l (0.000008 lb/gal).

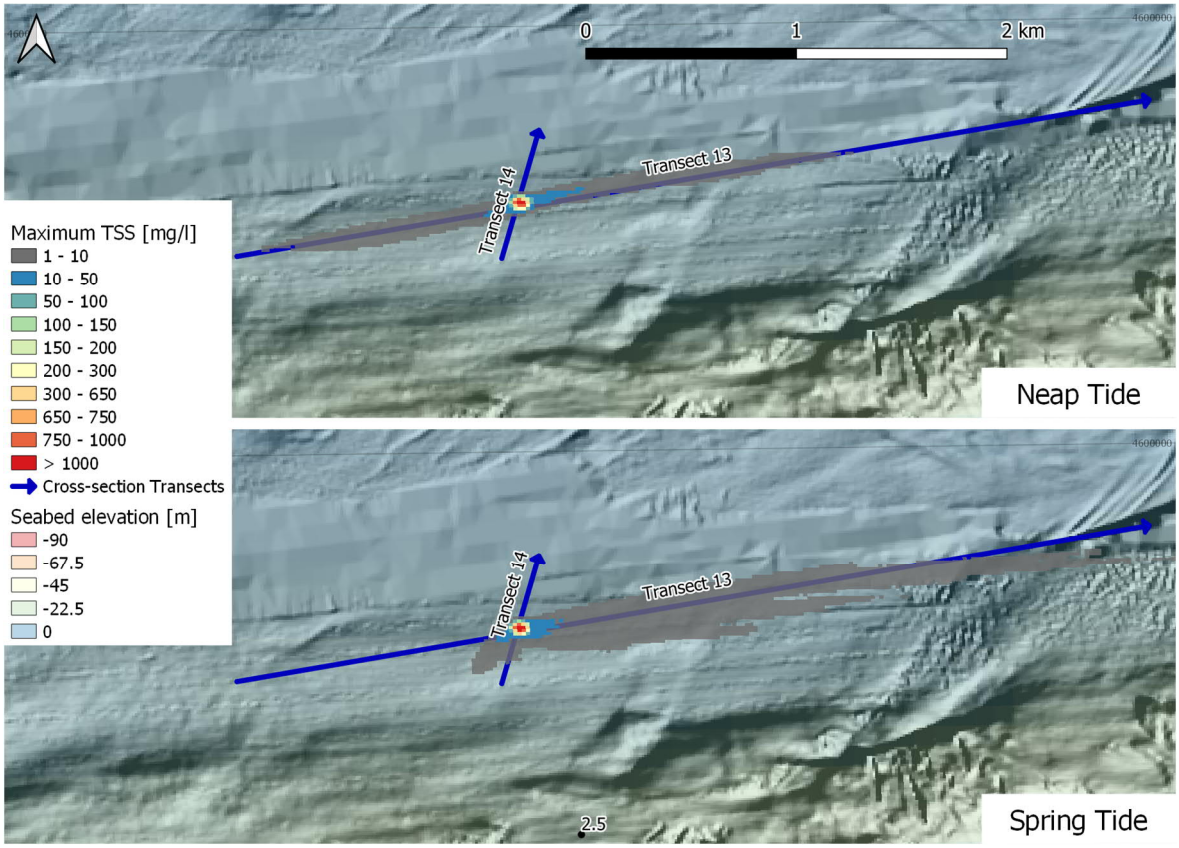

Figure 6.9: Map of maximum sediment concentration associated with HDD exit pit dredging, for Neap (up) and Spring (down) Tide conditions.

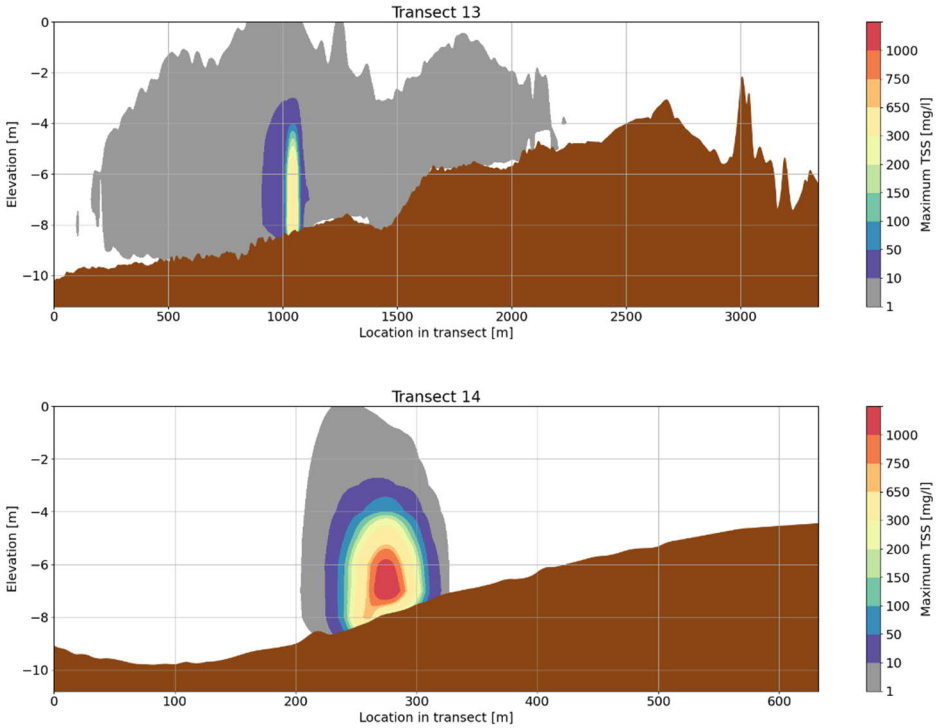

Figure 6.10: Vertical structure along selected transects of maximum sediment concentration associated with the HDD exit pit, Neap Tide scenario. The location of the associated transects is depicted in Figure 6.9.

Table 6.5: HDD exit pit, Neap Tide. Maximum distance and area for selected TSS thresholds.

TSS threshold [mg/l]	Maximum observed distance from release location [m]	Area exceeding TSS threshold [ha]
1	1200	18
10	230	1.7
50	45	0.53
100	36	0.39
150	32	0.35
200	28	0.30
300	27	0.24
650	20	0.14
750	20	0.14
1000	N/A	0.03

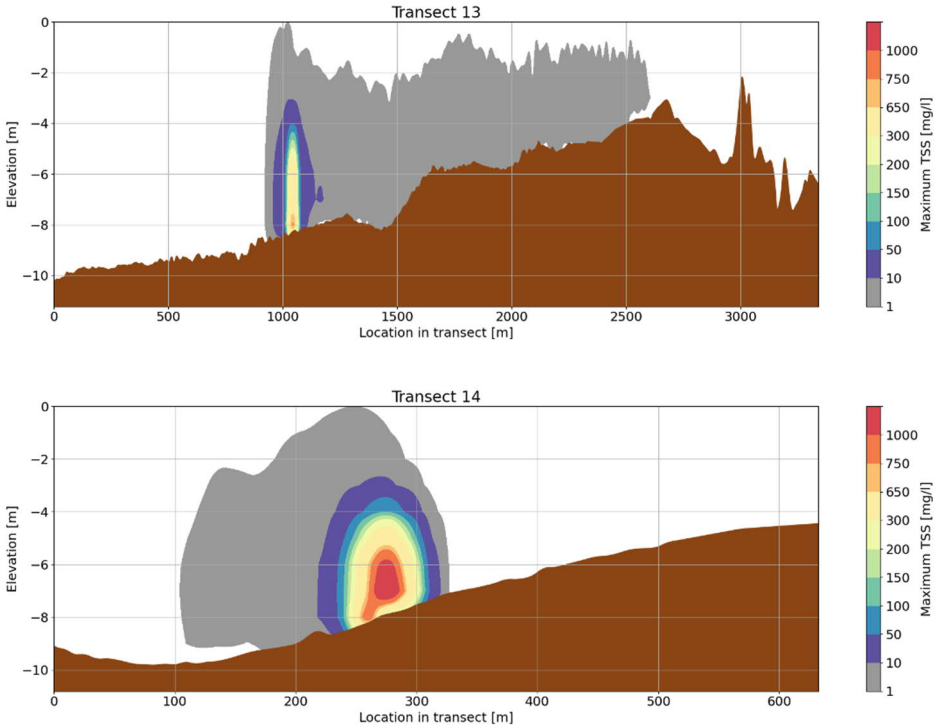

Figure 6.11: Vertical structure along selected transects of maximum sediment concentration associated with the HDD exit pit, Spring Tide scenario. The location of the associated transects is depicted in Figure 6.9.

Table 6.6: HDD exit pit, Spring Tide. Maximum distance and area for selected TSS thresholds.

TSS threshold [mg/l]	Maximum observed distance from release location [m]	Area exceeding TSS threshold [ha]
1	2519	37
10	150	1.5
50	39	0.48
100	35	0.35
150	34	0.36
200	28	0.30
300	27	0.26
650	20	0.14
750	20	0.14
1000	N/A	0.06

7 Sediment Plume Dispersion: Impact Duration

Sections 5 and 6 discussed the overall footprint of sediment deposition and TSS impacts associated with the installation activities. It is also interesting to understand how quickly the plume disperses to facilitate the assessment of the impact duration and its environmental consequences.

Table 7.1 shows, for each scenario, the time after the end of the release for the TSS to drop below selected levels. After two hours, the maximum TSS level drops below 10 mg/l (0.00008 lb/gal) for any of the simulated scenario. The maximum TSS level drops below 1 mg/l (0.000008 lb/gal) for any of the simulated scenario after less than four hours.

These results show that the TSS concentrations associated with the installation activities drop rapidly and last for a short time period only.

Table 7.1: Time for the TSS to drop below selected levels after the end of the release, for all scenarios.

Modelling Scenario	Time to drop below 100 mg/l [min]	Time to drop below 50 mg/l [min]	Time to drop below 10 mg/l [min]	Time to drop below 1 mg/l [min]
Segment 1	2.1	5.4	54.6	141.3
Segment 2	< 0.8	< 0.8	48.8	132.1
Segment 3	3.6	6.1	76.9	120.3
Inter-Array Cables	12.9	34.5	101.2	202.0
HDD exit pit, Neap Tide	< 0.8	< 0.8	< 0.8	9.6
HDD exit pit, Spring Tide	< 0.8	< 0.8	< 0.8	< 0.8

8 Discussions and Conclusions

The deposition of the sediment resulting from cable installation activities occurs relatively locally. Most of the released mass settles out quickly and is not transported for long distances by the currents. Deposition thicknesses exceeding 5 mm (0.2 inches) are generally limited to a corridor of maximum width 24 m (79 ft) around the cable corridor, although such thicknesses can be locally observed up to 180 m (591 ft) from the cable corridor. A larger amount of deposits tends to be observed in the vicinity of Segment 3 (KP 45 to KP 88) of the offshore export cables and of the inter-array cables, which is the consequence of the lower currents present in these areas resulting in less transport of sediment over long distances.

The impacted surface associated with the HDD exit pit dredging is very limited in terms of deposited sediment with deposits exceeding 5 mm (0.2 inches) found at respective maximum distances of 26 m (85 ft) and 32 m (105 ft) for the Neap and Spring Tide scenarios. However, in very close proximity to the HDD exit pit, the thickness of deposits exceeds 0.1 m (0.3 ft). Deposition thicknesses are greater if the location of the release is fixed. Trenching or dredging operations associated with cable laying are mobile, and thus will produce smaller maximum deposit thicknesses.

The observations of maximum TSS are correlated with the thickness of the deposits. Concentrations above 100 mg/l (0.0008 lb/gal) generally remain suspended around the corridor centerline. After two hours, the maximum TSS level drops below 10 mg/l (0.00008 lb/gal) for any of the simulated scenarios, while it drops below 1 mg/l (0.000008 lb/gal) after less than four hours. TSS levels above 100 mg/l (0.0008 lb/gal) are predicted to extend to a maximum of 370 m (1,214 ft) from the cable corridor centerlines and affect a cumulative area of 1,849 ha (4,569 ac) for the entirety of the offshore export cable corridors and inter-array cable routes. Further, the 150 mg/L (0.0013 lb/gal) contour is always within 250 m (820 ft) from the centerline. Observations of sediment concentrations exceeding 50 mg/l (0.00042 lb/gal) are generally limited to the first 5 m (16 ft) above the seabed, although they can attain 10 m (33 ft) above seabed in the case of the inter-array cables.

Turbidity levels associated with the HDD exit pit dredging are significantly smaller compared with the impact resulting from the cables trenching/dredging, with concentrations exceeding 100 mg/l (0.0008 lb/gal) found at a maximum distance of 36 m (118 ft) and affecting a cumulative area not exceeding 0.4 ha (1 ac).

TSS levels resulting from the installation operations can be compared with the natural background TSS levels. Figure 8.1 shows natural TSS levels resulting from the Metocean and Sediment Transport Modelling during the summer period. There are observed TSS values up to 1.1 mg/l (0.000008 lb/gal) for fine sand particles and 3.6 mg/l for very fine sand particles in the Muskeget Channel, resulting in a total amount of 4.7 mg/l for both very fine and fine sands. In the current study, TSS values in excess of 10 mg/l (0.00008 lb/gal) resulting from the

installation operations are found at maximum distances of 2,782 m (9,127 ft) from the source but are more generally observed within a 700-m (2,296-ft) corridor centered on the cable corridor. This slightly higher threshold of TSS compared to the natural background levels is then associated with a limited impacted area and over a short time period.

In summary, despite conservative model assumptions, seabed deposits and water quality impacts from cable installation and HDD exit pit dredging remain generally localized and of short duration.

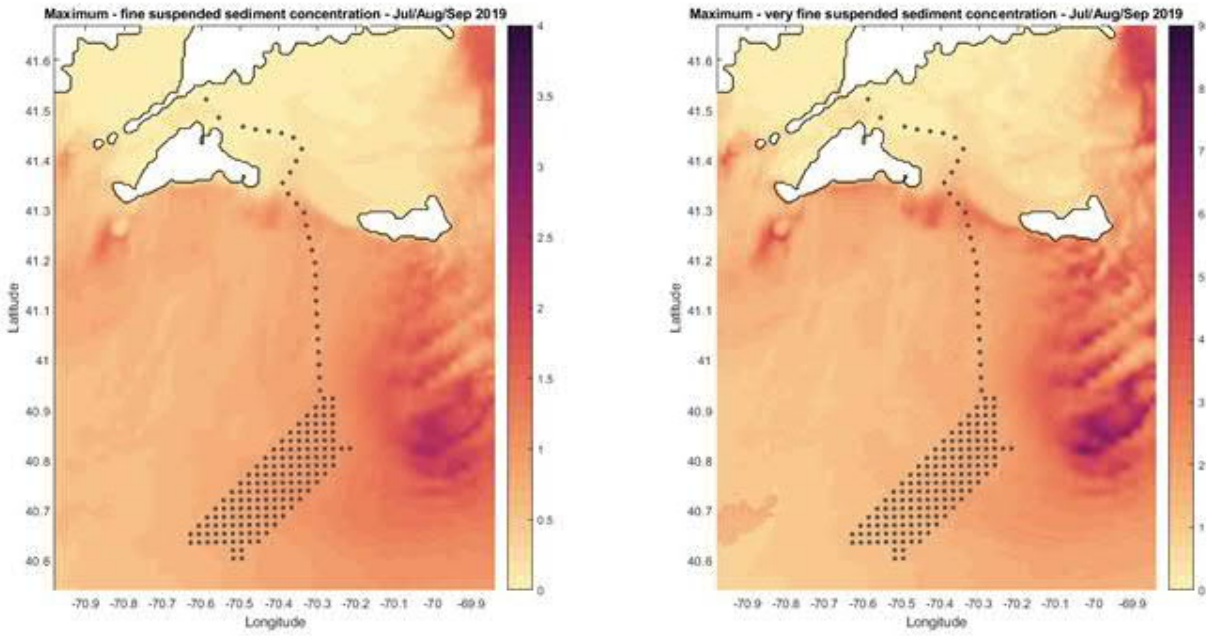

Figure 8.1: Maps of maximum near-bed TSS [mg/l] during the Jul/Aug/Sep 2019 period for fine sand (left) and very fine sand (right). Map resulting from the Metocean and Sediment Transport Modelling study (Fugro report No C170693 02 Metocean and Sediment Transport Modelling, 2020).

9 References

Alpha analytical, 2020a. Analytical report: MAYFLOWER SUMMER 2020. Project number 124560, lab number L2036591, serial number 9252017:01.

Alpha analytical, 2020b. Analytical report: MAYFLOWER SUMMER 2020. Project number 124560, lab number L2036615, serial number 09292009:35.

Alpha analytical, 2020c. Analytical report: MAYFLOWER SUMMER 2020. Project number 124560, lab number L2036622, serial number 09252017:36.

Alpha analytical, 2020d. Analytical report: MAYFLOWER SUMMER 2020. Project number 124560, lab number L2036657, serial number 09252017:36.

Booij, N., Ris, R.C., Holthuijsen, L.H. (1999). A third generation wave model for coastal regions, part I, model description and validation. Journal of Geophysical Research 104 (C4), 7649-7666.

Bureau of Ocean Energy Management (BOEM), 2020. Information Guidelines for a Renewable Energy Construction and Operations Plan (COP). Version 4.0: May 27, 2020. United States Department of the Interior. Sterling, VA

CERC (Coastal Engineering Research Center), 1984. Shore Protection Manual, Volume 1. US Army Corps of Engineers.

Chapman D., 1985. Numerical treament of cross-shelf open boundaries in a barotropic coastal ocean model, JPO, 15, 1060-1075.

Egbert, Gary D., Svetlana Y. Erofeeva, 2002. Efficient Inverse Modeling of Barotropic Ocean Tides. J. Atmos. Oceanic Technol., 19, 183–204.

Flather, R.A., 1976. A tidal model of the north-west European continental shelf. Memoires de la Societe Royale des Sciences de Liege 6 (10), 141–164.

Fugro report No. C170693 02, 2020. Metocean and Sediment Transport Modeling.

GEBCO Digital Atlas, 2003. British Oceanographic Data Centre on Behalf of IOC, IHO and BODC, Centenary Edition of the GEBCO Digital Atlas, published on CD-ROM on behalf of the Intergovernmental Oceanographic Commission and the International Hydrographic Organization as part of the General Bathymetric Chart of the Oceans, British Oceanographic Data Centre, Liverpool, U. K

Grant, W.D., Madsen, O.S., 1979. Combined wave and current interaction with a rough bottom. Journal of Geophysical Research 84 (C4), 1797-1808.

Jonsson, I.G. and N.A. Carlsen, 1976. Experimental and theoretical investigations in an oscillatory rough turbulent boundary layer. J. Hydr. Res., 14, 1, 45-60.

Khondaker, A.N., 2000. Modelling the fate of drilling waste in marine environment – an overview. Computers & Geosciences 26, 531-540.

Madsen, O.S., 1994. Spectral wave–current bottom boundary layer flows. In: Coastal Engineering 1994. Proceedings of the 24th International Conference on Coastal Engineering Research Council, Kobe, Japan, pp. 384–398.

Malarkey, J., Davies, A.G., 2003. A non-iterative procedure for the Wiberg and Harris (1994) oscillatory sand ripple predictor. Journal of Coastal Research 19 (3), 738–739.

Mellor, G.L., 2003. User's guide for a three-dimensional, primitive equation, numerical ocean model. Program in Atmospheric and Oceanic Sciences, Princeton University, Princeton, NJ 08544-0710.

Mellor, G.L., 2005. Some consequences of the three-dimensional currents and surface wave equations. Journal of Physical Oceanography 35, 2291–2298.

Mulligan, R. P., A. J. Bowen, A. E. Hay, A. J. van der Westhuysen, and J. A. Battjes, 2008. Whitecapping and wave field evolution in a coastal bay, J. Geophys. Res., 113, C03008, doi:10.1029/2007JC004382.

NOAA National Geophysical Data Center, 2009. ETOPO1 1 Arc-Minute Global Relief Model. NOAA National Centers for Environmental Information. Accessed in June 2020.

Nielsen, P., 1992. Coastal bottom boundary layers and sediment transport. World Scientific. Singapore, 324pp.

Padman L. and Erofeeva S., 2004. A barotropic inverse tidal model for the Artic Ocean, Geophysical Research Letters, vol. 31.

Soulsby R., 1995. Dynamics of marine sands, HR Wallingford, Thomas Telford Publications, pp 250.

Styles, R. and S.M. Glenn, 2000. Modeling stratified wave and current bottom boundary layers in the continental shelf, JGR, 105, 24119-24139.

Styles, R., Glenn, S.M., 2002. Modeling bottom roughness in the presence of wave-generated ripples. Journal of Geophysical Research 107 (C8), 24/1–24/15.

Tanaka, H., 1994. Development of a Prediction Scheme for Volcanic Ash Fall from Redoubt Volcano, Alaska. Proceedings of the First International Symposium on Volcanic Ash and Aviation Safety, U.S. Geological Survey, Bulletin 2047, 283-291.

Warner J.C., Sherwood C.R., Signell R.P., Harris C.K., Arango H.G., 2008. Development of a three dimensional, regional, coupled wave, current, and sediment transport model. Computers & Geosciences 34, 1284-1306.

Wiberg, P.L., Harris, C.K., 1994. Ripple geometry in wave dominated environments. Journal of Geophysical Research 99 (C1), 775–789.

Attachment A

Data Sources

A.1 Bathymetry

In this study, several bathymetric datasets were considered.

For the regional background, the public bathymetry from NCEI U.S. Coastal Relief Model, with a 3 arc-seconds resolution (70-90 m) is used (reference 1 below). Two other public datasets are also considered. A dataset from NOAA's National Geophysical Data Center covers the cable route, its surroundings and the northern part of the Lease Area with a resolution up to 10 m (reference 2 below). A 10 m resolution dataset built from data collected by the USGS, the National Oceanic and Atmospheric Administration, and the U.S. Army Corps of Engineers covers Vineyard Sound and western Nantucket Sound (reference 3). Information on these datasets is accessible through the following links:

- https://www.ngdc.noaa.gov/mgg/coastal/crm.html
- https://data.noaa.gov/metaview/page?xml=NOAA/NESDIS/NGDC/MGG/DEM//iso/xml/385.xml&view=getDataView&header=none#
- https://catalog.data.gov/dataset/10-m-bathymetry-grid-of-vineyard-and-western-nantucket-sounds-produced-from-lead-line-and-singl

In addition, this study uses two bathymetry datasets surveyed by Fugro:

- The first, a 0.5 m resolution gridded corridor aligned with the turbine locations.
- The second, available from the partially processed 2020 survey for the integrated geotechnical/geophysical interpretative study has a resolution of 0.25 m. This dataset partially covers the export cable corridors and some South-North oriented corridors aligned with the turbine locations.

A.2 Geotechnical data

The current study is based on Particles Size Distribution (PSD) of surface or shallow sub-surface as collected from grab samples. Two grab sampling surveys were considered: May 2020 (68 samples) and August 2020 (48 samples) to support both modelling and benthic habitat studies. These samples mostly cover the Lease Area as well as the offshore export cable corridor, Central Option. For each survey, classifications of the particle size distribution are available as percentages belonging to each of the following categories:

- Boulder (>256 mm)
- Cobbles (64-256 mm)
- Pebble (4-64 mm)
- Granule (2-4 mm)
- Very Coarse Sand
- Coarse Sand
- Medium Sand
- Fine Sand

- Very Fine Sand
- Silt (1.95-62.5 µm)
- Clay (<1.95 µm)

For the August 2020 benthic survey, reports by Alpha Analytical (2020a, 2020b, 2020c, 2020d) were available, providing values for the median particle diameters used in this study.

A.3 Metocean conditions

Metocean conditions used in this study including the description of currents and waves covering a period from July 1, 2018 to June 26, 2020 were extracted from time series of the dataset resulting from the coupled metocean modelling task (Section 3 and Attachment B).

A.4 Potential WTG/OSP(s) Locations

Table A.1: Potential WTG/OSP(s) Locations, including seabed elevation (MLLW) and (EPSG: 32619).

Name	Easting [m] WGS 84/UTM 19N	Northing [m] WGS 84/UTM 19N	Seabed elevation [m] MLLW
X47	393806	4530924	-37.75
Y47	393806	4529072	-38.86
X46	391954	4530924	-39.53
Z47	393806	4527220	-40.26
Y46	391954	4529072	-40.62
AD49	397510	4519812	-40.82
AA47	393806	4525368	-41.44
Y45	390102	4529072	-41.81
Z46	391954	4527220	-41.86
AD48	395658	4519812	-42.33
AB47	393806	4523516	-42.95
AA46	391954	4525368	-43.01
Z45	390102	4527220	-43.19
AC47	393806	4521664	-43.28
AD47	393806	4519812	-43.53
AB46	391954	4523516	-43.90
AF47	393806	4516108	-43.93
AA45	390102	4525368	-43.99
AC46	391954	4521664	-44.05
AE47	393806	4517960	-44.05
Z44	388250	4527220	-44.12
AF46	391954	4516108	-44.29
AB45	390102	4523516	-44.52
AC45	390102	4521664	-44.60

Name	Easting [m] WGS 84/UTM 19N	Northing [m] WGS 84/UTM 19N	Seabed elevation [m] MLLW
AA44	388250	4525368	-44.74
AF45	390102	4516108	-44.75
AE46	391954	4517960	-44.76
AD46	391954	4519812	-44.82
AG46	391954	4514256	-44.87
AE45	390102	4517960	-45.09
AB44	388250	4523516	-45.72
AE44	388250	4517960	-45.73
AA43	386398	4525368	-45.84
AD45	390102	4519812	-45.85
AG45	390102	4514256	-46.30
AE43	386398	4517960	-46.31
AF44	388250	4516108	-46.61
AC44	388250	4521664	-46.79
AH45	390102	4512404	-47.28
AB43	386398	4523516	-47.39
AD44	388250	4519812	-47.46
AF43	386398	4516108	-47.51
AI43	386398	4510552	-47.57
AG44	388250	4514256	-47.73
AD43	386398	4519812	-47.86
AI44	388250	4510552	-47.86
AC43	386398	4521664	-48.01
AD42	384546	4519812	-48.28
AI42	384546	4510552	-48.37
AJ43	386398	4508700	-48.45
AH44	388250	4512404	-48.45
AE42	384546	4517960	-48.48
AB42	384546	4523516	-48.61
AG43	386398	4514256	-48.77
AF42	384546	4516108	-48.78
AH42	384546	4512404	-48.88
AJ42	384546	4508700	-48.88
AC42	384546	4521664	-48.93
AH43	386398	4512404	-49.00
AD40	380842	4519812	-49.10

Name	Easting [m] WGS 84/UTM 19N	Northing [m] WGS 84/UTM 19N	Seabed elevation [m] MLLW
AE41	382694	4517960	-49.37
AC41	382694	4521664	-49.42
AI41	382694	4510552	-49.44
AD41	382694	4519812	-49.60
AH41	382694	4512404	-49.68
AG42	384546	4514256	-50.01
AH40	380842	4512404	-50.08
AI40	380842	4510552	-50.20
AJ41	382694	4508700	-50.29
AG40	380842	4514256	-50.38
AG41	382694	4514256	-50.52
AK42	384546	4506848	-50.53
AF41	382694	4516108	-50.57
AG39	378990	4514256	-50.67
AF39	378990	4516108	-50.71
AH39	378990	4512404	-50.93
AF38	377138	4516108	-50.95
AE40	380842	4517960	-51.17
AJ40	380842	4508700	-51.20
AK41	382694	4506848	-51.21
AG38	377138	4514256	-51.37
AI39	378990	4510552	-51.42
AG37	375286	4514256	-51.52
AH38	377138	4512404	-51.53
AF40	380842	4516108	-51.57
AI38	377138	4510552	-51.78
AK40	380842	4506848	-51.93
AJ39	378990	4508700	-52.09
AL41	382694	4504996	-52.20
AJ38	377138	4508700	-52.48
AH37	375286	4512404	-52.59
AE39	378990	4517960	-52.62
AL40	380842	4504996	-52.81
AI37	375286	4510552	-52.86
AK39	378990	4506848	-52.89
AI36	373434	4510552	-53.21

Name	Easting [m] WGS 84/UTM 19N	Northing [m] WGS 84/UTM 19N	Seabed elevation [m] MLLW
AJ37	375286	4508700	-53.33
AK38	377138	4506848	-53.57
AL39	378990	4504996	-53.62
AH36	373434	4512404	-53.91
AM40	380842	4503144	-53.93
AM39	378990	4503144	-54.28
AL38	377138	4504996	-54.41
AK37	375286	4506848	-54.41
AJ36	373434	4508700	-54.52
AI35	371582	4510552	-54.98
AL37	375286	4504996	-55.02
AK36	373434	4506848	-55.07
AM38	377138	4503144	-55.19
AJ35	371582	4508700	-55.42
AL36	373434	4504996	-55.69
AK35	371582	4506848	-55.88
AM35	371582	4503144	-56.25
AM37	375286	4503144	-56.36
AL35	371582	4504996	-56.50
AN39	378990	4501292	-56.73
AM36	373434	4503144	-56.75
AJ34	369730	4508700	-56.80
AK34	369730	4506848	-56.88
AN38	377138	4501292	-57.06
AK33	367878	4506848	-57.15
AL34	369730	4504996	-57.40
AL33	367878	4504996	-57.75
AN37	375286	4501292	-57.97
AM33	367878	4503144	-58.53
AM34	369730	4503144	-58.54
AN35	371582	4501292	-58.75
AO38	377138	4499440	-58.78
AN34	369730	4501292	-58.80
AN36	373434	4501292	-58.83
AL32	366026	4504996	-58.89
AN33	367878	4501292	-58.96

Name	Easting [m] WGS 84/UTM 19N	Northing [m] WGS 84/UTM 19N	Seabed elevation [m] MLLW
AO37	375286	4499440	-59.10
AO36	373434	4499440	-59.41
AM32	366026	4503144	-59.59
AN31	364174	4501292	-60.01
AN32	366026	4501292	-60.12
AO35	371582	4499440	-60.48
AO33	367878	4499440	-60.50
AO34	369730	4499440	-60.50
AO32	366026	4499440	-60.62
AM31	364174	4503144	-60.65
AO31	364174	4499440	-60.94
AP36	373434	4497588	-61.00
AN30	362322	4501292	-61.08
AP35	371582	4497588	-61.21
AO30	362322	4499440	-61.43
AQ36	373434	4495736	-62.47
AQ35	371582	4495736	-62.70

A.5 Grab sample stations

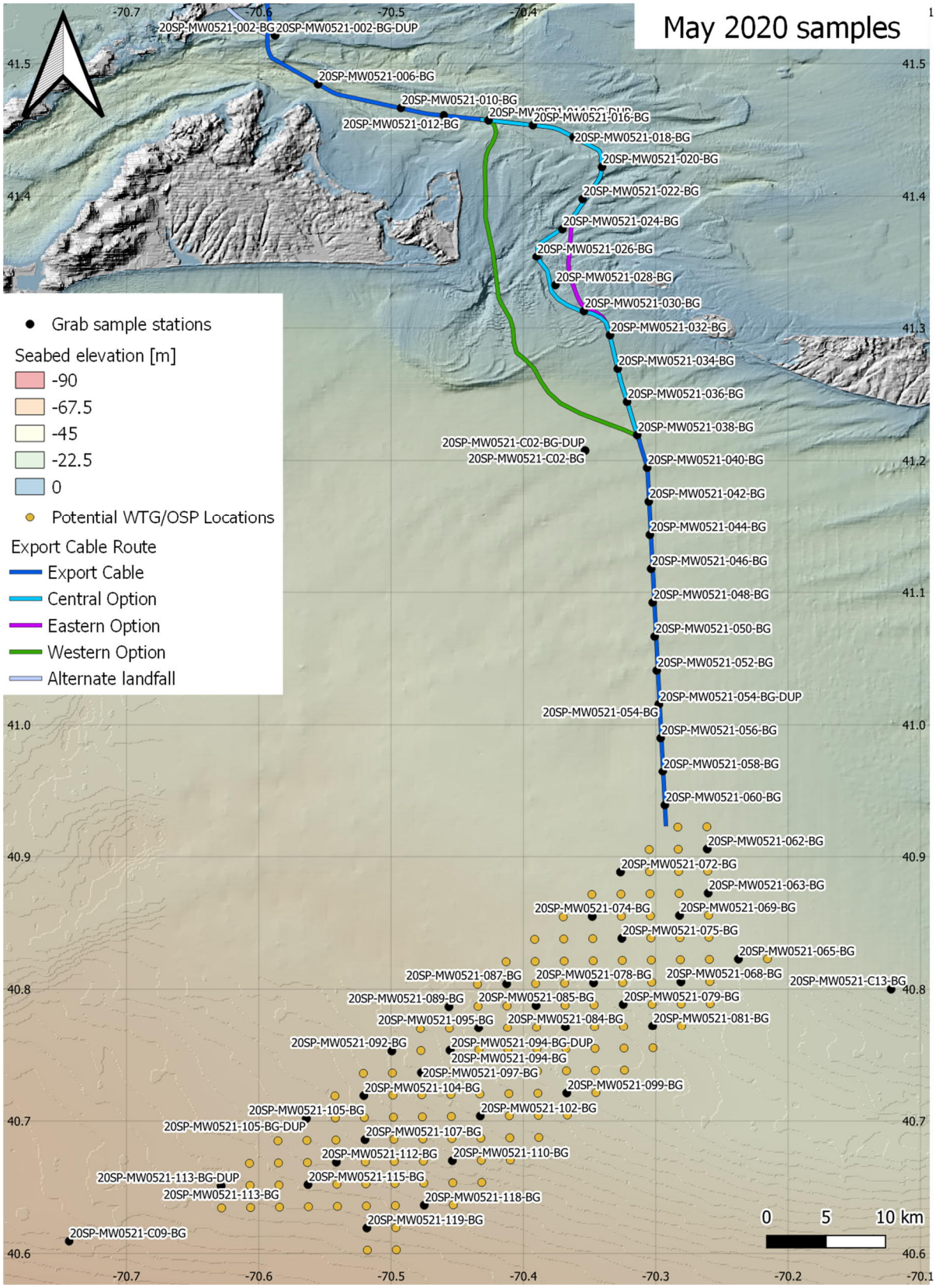

Figure A.1: Grab sample stations corresponding to Table A.2 (May 2020 samples).

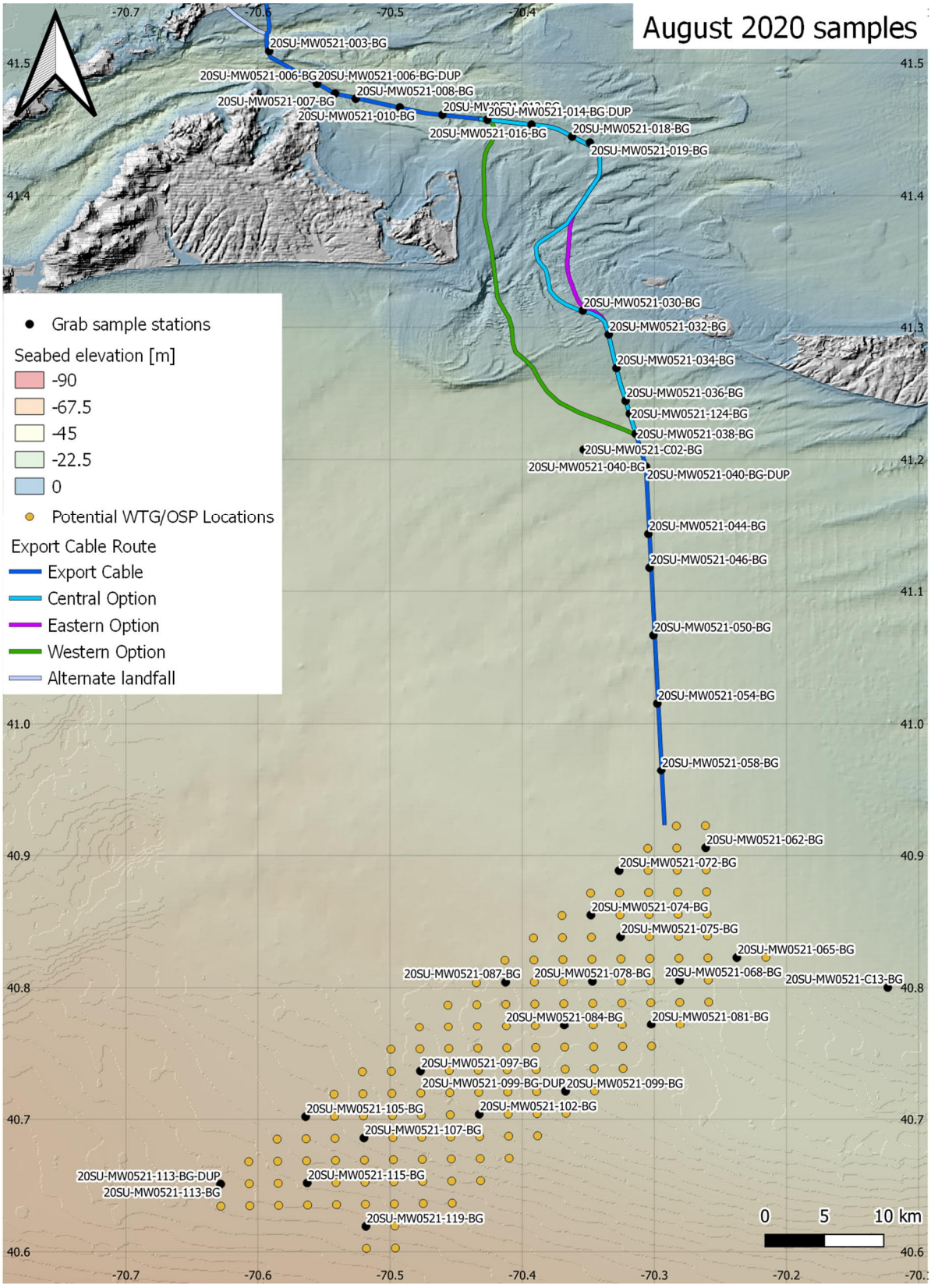

Figure A.2: Grab sample stations corresponding to Table A.3 (August 2020 samples).

Table A.2: Grab sample stations for May 2020 survey, with coordinates in the NAD 83/UTM 19N coordinates system (EPSG: 26919).

Sample ID	Easting [m] NAD 83/UTM 19N	Northing [m] NAD 93/UTM 19N
20SP-MW0521-002-BG	367534	4597861
20SP-MW0521-006-BG	370177	4593729
20SP-MW0521-010-BG	375374	4591645
20SP-MW0521-012-BG	378066	4590977
20SP-MW0521-014-BG	380881	4590524
20SP-MW0521-016-BG	383675	4590060
20SP-MW0521-018-BG	386229	4589016
20SP-MW0521-020-BG	387985	4586492
20SP-MW0521-022-BG	386720	4583826
20SP-MW0521-024-BG	385398	4581320
20SP-MW0521-026-BG	383728	4579019
20SP-MW0521-028-BG	384883	4576582
20SP-MW0521-030-BG	386653	4574372
20SP-MW0521-032-BG	388274	4572331
20SP-MW0521-034-BG	388721	4569515
20SP-MW0521-036-BG	389268	4566735
20SP-MW0521-038-BG	389867	4563940
20SP-MW0521-040-BG	390454	4561182
20SP-MW0521-042-BG	390517	4558349
20SP-MW0521-044-BG	390544	4555502
20SP-MW0521-046-BG	390580	4552652
20SP-MW0521-048-BG	390636	4549824
20SP-MW0521-050-BG	390720	4546977
20SP-MW0521-052-BG	390810	4544130
20SP-MW0521-054-BG	390903	4541293
20SP-MW0521-056-BG	390975	4538457
20SP-MW0521-058-BG	391061	4535626
20SP-MW0521-060-BG	391157	4532782
20SP-MW0521-062-BG	393800	4529062
20SP-MW0521-063-BG	393808	4525375
20SP-MW0521-065-BG	395658	4519813
20SP-MW0521-068-BG	391968	4517955
20SP-MW0521-069-BG	391955	4523523

Sample ID	Easting [m] NAD 83/UTM 19N	Northing [m] NAD 93/UTM 19N
20SP-MW0521-072-BG	388248	4527218
20SP-MW0521-074-BG	386395	4523519
20SP-MW0521-075-BG	388249	4521661
20SP-MW0521-078-BG	386393	4517960
20SP-MW0521-079-BG	388253	4516118
20SP-MW0521-081-BG	390106	4514271
20SP-MW0521-084-BG	384537	4514268
20SP-MW0521-085-BG	382697	4516118
20SP-MW0521-087-BG	380855	4517969
20SP-MW0521-089-BG	377140	4516102
20SP-MW0521-092-BG	373430	4512393
20SP-MW0521-094-BG	377153	4512399
20SP-MW0521-095-BG	379003	4514267
20SP-MW0521-097-BG	375293	4510546
20SP-MW0521-099-BG	384537	4508699
20SP-MW0521-102-BG	378986	4506855
20SP-MW0521-104-BG	371582	4508686
20SP-MW0521-105-BG	367878	4506831
20SP-MW0521-107-BG	371593	4504999
20SP-MW0521-110-BG	377142	4503144
20SP-MW0521-112-BG	369724	4503143
20SP-MW0521-113-BG	362329	4501282
20SP-MW0521-115-BG	367883	4501292
20SP-MW0521-118-BG	375281	4499444
20SP-MW0521-119-BG	371580	4497600
20SP-MW0521-002-BG-DUP	367534	4597861
20SP-MW0521-014-BG-DUP	380881	4590524
20SP-MW0521-054-BG-DUP	390903	4541293
20SP-MW0521-094-BG-DUP	377153	4512399
20SP-MW0521-105-BG-DUP	367878	4506831
20SP-MW0521-113-BG-DUP	362329	4501282
20SP-MW0521-C02-BG	386544	4562685
20SP-MW0521-C02-BG-DUP	386544	4562685
20SP-MW0521-C09-BG	352523	4496842
20SP-MW0521-C13-BG	405360	4517157

Table A.3: Grab sample stations for August 2020 survey, with coordinates in the NAD 83/UTM 19N coordinates system (EPSG: 26919).

Sample ID	Easting [m] NAD 83/UTM 19N	Northing [m] NAD 83/UTM 19N
20SU-MW0521-003-BG	367191	4596510
20SU-MW0521-006-BG	370168	4593728
20SU-MW0521-006-BG-DUP	370168	4593728
20SU-MW0521-007-BG	371287	4592880
20SU-MW0521-008-BG	372587	4592423
20SU-MW0521-009-BG	372587	4592423
20SU-MW0521-010-BG	375362	4591650
20SU-MW0521-012-BG	378047	4590980
20SU-MW0521-014-BG	380875	4590522
20SU-MW0521-014-BG-DUP	380875	4590522
20SU-MW0521-016-BG	383664	4590062
20SU-MW0521-018-BG	386216	4589019
20SU-MW0521-019-BG	387335	4588506
20SU-MW0521-030-BG	386664	4574363
20SU-MW0521-032-BG	388277	4572332
20SU-MW0521-034-BG	388723	4569501
20SU-MW0521-036-BG	389263	4566744
20SU-MW0521-038-BG	389865	4563956
20SU-MW0521-040-BG	390463	4561185
20SU-MW0521-040-BG-DUP	390463	4561185
20SU-MW0521-044-BG	390538	4555483
20SU-MW0521-046-BG	390572	4552653
20SU-MW0521-050-BG	390733	4546989
20SU-MW0521-054-BG	390895	4541274
20SU-MW0521-058-BG	391058	4535627
20SU-MW0521-062-BG	393796	4529067
20SU-MW0521-065-BG	395654	4519824
20SU-MW0521-068-BG	391972	4517948
20SU-MW0521-072-BG	388247	4527238
20SU-MW0521-074-BG	386386	4523533
20SU-MW0521-075-BG	388259	4521673
20SU-MW0521-078-BG	386402	4517952
20SU-MW0521-081-BG	390104	4514264
20SU-MW0521-084-BG	384546	4514273
20SU-MW0521-087-BG	380865	4517979

Sample ID	Easting [m] NAD 83/UTM 19N	Northing [m] NAD 83/UTM 19N
20SU-MW0521-097-BG	375294	4510544
20SU-MW0521-099-BG	384539	4508716
20SU-MW0521-099-BG-DUP	384539	4508716
20SU-MW0521-102-BG	378987	4506867
20SU-MW0521-105-BG	367888	4506846
20SU-MW0521-107-BG	371582	4505000
20SU-MW0521-113-BG	362345	4501293
20SU-MW0521-113-BG-DUP	362345	4501293
20SU-MW0521-115-BG	367891	4501290
20SU-MW0521-119-BG	371580	4497587
20SU-MW0521-124-BG	389515	4565658
20SU-MW0521-C02-BG	386538	4562681
20SU-MW0521-C13-BG	405258	4517172

A.6 Offshore export cable corridor coordinates associated with the construction scenarios

Table A.4: Offshore export cable corridor, KP 0 to KP 20. Corridor coordinates in NAD 83/UTM 19N (EPSG: 26919) coordinate system. Seabed elevations were obtained from the NCEI U.S. Coastal Relief Model dataset (see Attachment A)

KP [km]	Easting [m] NAD 83/UTM 19N	Northing [m] NAD 83/UTM 19N	Seabed elevation [m] MLLW
0	367013	4600647	1.01
0.88	367136	4599772	-4.37
1.41	367208	4599250	-7.39
1.94	367279	4598728	-11.6
2.36	367367	4598311	-20.31
2.69	367493	4598008	-21.79
2.87	367528	4597830	-17.92
3.11	367524	4597592	-8.24
3.5	367474	4597208	-11.77
3.94	367309	4596795	-16.68
4.19	367182	4596585	-14.76
4.69	367137	4596090	-14.93
5.55	367824	4595559	-20.89
6.42	368511	4595028	-24.37
7.29	369199	4594497	-23.74
8.16	369886	4593965	-22.23
9.03	370573	4593434	-22.43
9.9	371261	4592903	-22.75
10.88	372195	4592615	-22.98
11.85	373129	4592327	-19.57
12.83	374063	4592040	-19.26
13.81	374997	4591752	-17.75
14.78	375931	4591464	-16.11
15.76	376865	4591176	-16.83
16.76	377851	4591015	-16.95
17.76	378838	4590855	-20.44
18.76	379824	4590694	-18.67
19.76	380811	4590534	-20.96
20	381048	4590495	-21.11

Table A.5: Offshore export cable corridor, KP 20 to KP 45. Corridor coordinates in NAD 83/UTM 19N (EPSG: 26919). Seabed elevations were obtained from the NCEI U.S. Coastal Relief Model dataset (see Attachment A)

KP [km]	Easting [m] NAD 83/UTM 19N	Northing [m] NAD 83/UTM 19N	Seabed elevation [m] MLLW
20	381048	4590495	-21.11
20.76	381797	4590373	-20.17
21.76	382784	4590213	-19.4
22.76	383770	4590052	-19.15
23.76	384757	4589892	-21.11
24.24	385218	4589749	-21.45
25.07	385896	4589267	-19.12
25.9	386574	4588785	-19.46
26.74	387252	4588303	-21.32
27.57	387930	4587821	-16.94
28.56	387951	4586831	-8.75
29.55	387972	4585842	-8.13
30.5	387521	4585003	-9.41
31.45	387070	4584163	-13.61
32.41	386619	4583323	-9.36
33.36	386167	4582484	-9.33
34.31	385716	4581644	-13.44
35.22	385024	4581066	-13.46
36.12	384332	4580487	-12.32
36.51	384023	4580241	-12.69
36.83	383829	4579995	-13.05
36.91	383818	4579913	-11.57
37.17	383781	4579653	-10.1
37.45	383798	4579377	-6.31
37.85	383830	4578975	-6.5
38.1	383884	4578735	-9.7
38.88	384249	4578038	-11.46
39.24	384385	4577707	-10.9
39.72	384495	4577242	-9.71
40.22	384504	4576746	-11
40.84	384609	4576127	-7.12
41.23	384755	4575768	-6.33
41.76	385052	4575327	-6.01
42.61	385727	4574814	-5.23
43.42	386428	4574404	-5.31

KP [km]	Easting [m] NAD 83/UTM 19N	Northing [m] NAD 83/UTM 19N	Seabed elevation [m] MLLW
44.25	387210	4574142	-6.39
44.99	387807	4573701	-7.12
45	387813	4573692	-7.28

Table A.6: Offshore export cable corridor, KP 45 to KP 88. Corridor coordinates in NAD 83/UTM 19N (EPSG: 26919). Seabed elevations were obtained from the NCEI U.S. Coastal Relief Model dataset (see Attachment A)

KP [km]	Easting [m] NAD 83/UTM 19N	Northing [m] NAD 83/UTM 19N	Seabed elevation [m] MLLW
45	387813	4573692	-7.28
45.64	388148	4573150	-6.92
46.5	388283	4572296	-6.31
47.37	388418	4571441	-8.24
48.23	388553	4570586	-10.74
49.1	388688	4569732	-13.8
49.96	388822	4568877	-17.06
50.96	389029	4567906	-20.95
51.95	389236	4566936	-21.88
52.94	389443	4565965	-24.83
53.93	389650	4564994	-26.92
54.93	389857	4564023	-25.92
55.92	390063	4563053	-27.24
56.91	390270	4562082	-27.73
57.9	390477	4561111	-27.54
58.9	390501	4560114	-30.09
59.9	390525	4559117	-29.81
60.9	390549	4558120	-29.42
61.89	390574	4557123	-29.66
62.89	390598	4556126	-31.96
63.89	390622	4555129	-31.08
64.88	390646	4554132	-30.84
65.88	390670	4553135	-32.63
66.88	390694	4552138	-33.42
67.88	390718	4551141	-33.77
68.87	390742	4550144	-34.07
69.87	390766	4549147	-34.38
70.87	390790	4548150	-34.27
71.87	390814	4547153	-33.03
72.86	390839	4546155	-34.24
73.86	390863	4545158	-35.21
74.86	390887	4544161	-35.25
75.85	390911	4543164	-36.23
76.85	390935	4542167	-37.02
77.85	390959	4541170	-37.14

KP [km]	Easting [m] NAD 83/UTM 19N	Northing [m] NAD 83/UTM 19N	Seabed elevation [m] MLLW
78.85	390983	4540173	-37.26
79.84	391007	4539176	-37.99
80.84	391031	4538179	-38.41
81.84	391055	4537182	-38.72
82.84	391080	4536185	-38.56
83.83	391104	4535188	-38.38
84.83	391128	4534191	-38.38
85.83	391152	4533194	-38.83
86.83	391176	4532197	-39.37
87.82	391200	4531200	-39.81

Table A.7: Inter-array cable route. Route coordinates in coordinates system NAD 83/UTM 19N (EPSG: 26919). Seabed elevations were obtained from the NCEI U.S. Coastal Relief Model dataset (see Attachment A)

KP [km]	Easting [m] NAD 83/UTM 19N	Northing [m] NAD 83/UTM 19N	Seabed elevation [m] MLLW
0	391175	4531135	-39.97
0.97	391062	4530177	-40.52
1.93	390949	4529218	-41.31
2.9	390836	4528259	-42.18
3.86	390723	4527300	-43.01
4.83	390610	4526341	-43.58
5.79	390497	4525382	-43.92
6.76	390384	4524423	-44.5
7.72	390271	4523464	-44.64
8.69	389561	4522804	-45.22
9.66	388852	4522144	-46.06
10.63	388143	4521484	-46.9
11.6	387433	4520824	-47.5
12.57	386724	4520164	-47.9
13.54	386014	4519504	-47.85
14.51	385305	4518844	-47.82
15.48	384596	4518184	-48.3
16.45	383886	4517524	-49.37
17.41	383177	4516864	-49.71
18.38	382467	4516204	-50.52
19.35	381758	4515544	-50.9
20.32	381049	4514884	-50.6
21.29	380339	4514224	-50.5
22.26	379630	4513564	-50.6
23.23	378920	4512904	-51
24.2	378211	4512244	-51.05
25.17	377502	4511584	-51.4
26.13	376792	4510924	-51.9
27.1	376083	4510264	-52.42
28.07	375373	4509604	-53.01
29.04	374664	4508944	-53.7
30.01	373954	4508284	-54.39
30.98	373245	4507624	-54.95
31.95	372382	4507172	-55.59
32.93	371519	4506720	-56.04

KP [km]	Easting [m] NAD 83/UTM 19N	Northing [m] NAD 83/UTM 19N	Seabed elevation [m] MLLW
33.84	371586	4505813	-56.34
34.75	371653	4504906	-56.63
35.71	371636	4503945	-57.19
36.67	371619	4502984	-57.65
37.57	371630	4502078	-58.51
38.48	371642	4501172	-59.02
39.44	371597	4500211	-59.97
40.4	371552	4499251	-60.6
41.34	371590	4498316	-61
42.27	371629	4497382	-61.47
43.13	371613	4496530	-62.1
43.98	371598	4495679	-62.63

Attachment B

Metocean Models

B.1 Numerical Models

The set of models used is the Coupled Ocean-Atmosphere-Wave-Sediment Transport (COAWST) Modelling System. COAWST is a model coupling toolkit to exchange data fields between the hydrodynamic currents model (ROMS), an atmospheric model like WRF (not employed in this study), the wave model (SWAN), and sediment capabilities of the Community Sediment Transport Model (not employed in this study).

B.2 Wave Model (SWAN)

The SWAN model (Booij et al, 1999) is a third generation shallow-water spectral wave model that includes wave propagation, refraction due to currents and depth, generation by wind, dissipation (white capping, bottom friction, depth-induced breaking), and nonlinear wave-wave interactions. SWAN is widely used to simulate wave conditions in coastal areas, where propagation, wave generation and dissipation processes are represented as: refraction and shoaling, reflection, diffraction, bottom friction, ambient currents, and depth induced breaking. The wave model solves the action balance equation as action density is conserved in the presence of currents. SWAN allows input of time and spatial varying ocean currents and water level.

The model conserves wave action density $N(\sigma,\theta)$, equal to energy density $E(\sigma,\theta)$, divided by the relative wave frequency σ. The relative wave frequency σ is related to the fixed wave frequency ω by the wave number vector k and mean current vector u,

$$\sigma = \omega - \boldsymbol{k}\cdot\boldsymbol{u} \qquad (3.1)$$

The evolution of the wave field in SWAN is described by the action balance equation

$$\frac{\partial}{\partial t}N + \frac{\partial}{\partial x}(c_x)N + \frac{\partial}{\partial y}(c_y)N + \frac{\partial}{\partial \sigma}c_\sigma N + \frac{\partial}{\partial \theta}c_\theta N = \frac{S_{tot}}{\sigma} \qquad (3.2)$$

The left side of this equation contains propagation terms in both geographical and spectral space (refraction is considered as propagation in spectral space). The right side of the equation contains source terms which model the generation and dissipation of wave energy.

In Equation (3.2) $N(\sigma,\theta;x,y,t)$ is the action density as a function of intrinsic frequency σ, direction θ, horizontal coordinates x and y, and time t. The first term on the left-hand side represents the local rate of change of action density in time, the second and third terms represent the propagation of action in geographical x, y space, respectively; propagation velocities c_x and c_y. The fourth term represents shifting of the relative frequency due to variations in depths and currents, with propagation velocity c_σ in σ space. The fifth term represents depth and current-induced refraction, with propagation velocity c_θ in θ space. All these expressions are taken from the linear wave theory and the diffraction is not included in the model. The term $S_{tot}(\sigma,\theta;x,y,t)$ at the righ-hand side of the action balance equation is

the source term representing the effects of generation, dissipation, and nonlinear wave-wave interactions (Booij et al, 1999). Radiation stresses are determined from spatial gradients in the directional energy spectrum $E(\sigma,\theta)$. The strongest gradients in radiation stress occur owing to depth-induced breaking (Mulligan et al, 2008).

B.3 Ocean Model (ROMS)

The ocean model is the Regional Ocean Modelling System (ROMS), a general class of free surface, terrain-following numerical models that solve the three-dimensional Reynolds-averaged Navier-Stokes equations (RANS) using the hydrostatic and Boussinesq approximations. ROMS uses finite-differences approximations on a horizontal curvilinear Arakawa C grid and on a vertical stretched terrain-following coordinate. Momentum and scalar advection and diffusive processes are solved using transport equations and an equation of state computes the density field that accounts for temperature, salinity, and suspended-sediment contributions.

In COAWST the ROMS model has been modified to include wave induced momentum flux (horizontal and vertical wave radiation stresses) that are important in near-shore regions by adding depth dependent radiation stress terms in the three-dimensional momentum equations and depth-independent terms to the two-dimensional momentum equations.

The governing equations in Cartesian coordinates are:

$$\frac{\partial(H_z u)}{\partial t}+\frac{\partial(uH_z u)}{\partial x}+\frac{\partial(vH_z u)}{\partial y}+\frac{\partial(\Omega H_z u)}{\partial s}-fH_z v = -\frac{H_z}{\rho_0}\frac{\partial p}{\partial x}-H_z g\frac{\partial \eta}{\partial x}-\frac{\partial}{\partial s}\left(\overline{u'w'}-\frac{\nu}{H_z}\frac{\partial u}{\partial s}\right)-\frac{\partial(H_z S_{xx})}{\partial x}-\frac{\partial\left(H_z S_{xy}\right)}{\partial y}+\frac{\partial S_{px}}{\partial s} \tag{3.3}$$

$$\frac{\partial(H_z v)}{\partial t}+\frac{\partial(uH_z v)}{\partial x}+\frac{\partial(vH_z v)}{\partial y}+\frac{\partial(\Omega H_z v)}{\partial s}+fH_z u = -\frac{H_z}{\rho_0}\frac{\partial p}{\partial y}-H_z g\frac{\partial \eta}{\partial y}-\frac{\partial}{\partial s}\left(\overline{v'w'}-\frac{\nu}{H_z}\frac{\partial v}{\partial s}\right)-\frac{\partial\left(H_z S_{xy}\right)}{\partial x}-\frac{\partial\left(H_z S_{yy}\right)}{\partial y}+\frac{\partial S_{py}}{\partial s} \tag{3.4}$$

$$0 = -\frac{1}{\rho_0}\frac{\partial p}{\partial s}-\frac{g}{\rho_0}H_z\rho \tag{3.5}$$

with continuity as:

$$\frac{\partial \eta}{\partial t}+\frac{\partial(H_z u)}{\partial x}+\frac{\partial(H_z v)}{\partial y}+\frac{\partial(H_z \Omega)}{\partial s}=0 \tag{3.6}$$

and scalar transport:

$$\frac{\partial(H_z C)}{\partial t} + \frac{\partial(uH_z C)}{\partial x} + \frac{\partial(vH_z C)}{\partial y} + \frac{\partial(\Omega H_z C)}{\partial s} = -\frac{\partial}{\partial s}\left(\overline{c'w'} - \frac{\nu_\theta}{H_z}\frac{\partial C}{\partial s}\right) + C_{source} \quad (3.7)$$

The equations are closed by parameterizing the Reynolds stresses and turbulent tracer fluxes as:

$$\overline{u'w'} = -K_M \frac{\partial u}{\partial z}; \quad \overline{v'w'} = -K_M \frac{\partial v}{\partial z}; \quad \overline{c'w'} = -K_c \frac{\partial c}{\partial z}; \quad (3.8)$$

where, u, v, and Ω are the mean components in the horizontal (x and y) and vertical (s) directions respectively; the vertical sigma coordinate $s = (z - \eta)/D$ ranges from s=-1 at the bottom to s=0 at the free surface; z is the vertical coordinate positive upwards with z=0 at mean sea level; η is the wave-averaged free surface elevation; D is the total water depth D=h+η; h is the depth below mean sea level of the sea floor; H_z is the grid cell thickness; f is the Coriolis parameter. An overbar represents a time average, and a prime (') represents turbulent fluctuations. K_M, K_c is vertical eddy viscosity and diffusivity; Pressure is p; ρ and ρ_0 are total and reference densities for seawater; g is acceleration due to gravity; ν and ν_θ are molecular viscosity and diffusivity; S_{xx}, S_{xy}, S_{yy} represent horizontal radiation stress; S_{py}, S_{px} represent vertical radiation stress; C represents a tracer quantity (e.g. salt, temperature, suspended sediment); C_{source} are tracer source/sink terms; and a function $\rho = f(C)$ is required to close the density relation. These equations are closed by parameterizing the Reynolds stress using one of the five options for turbulent-closure models in ROMS (Warner et al, 2008).

In Equations (3.3) and (3.4) the terms on the left hand side are: the change rate, horizontal advection and vertical advection, and the Coriolis parameter; on the right hand side: baroclinic gradient, surface pressure gradient, vertical viscosity, horizontal radiation and vertical radiation (where the surface roller term is included). Equation (3.5) represents the hydrostatic buoyancy force, Equation (3.6) represents the continuity equation and the equation (3.7) represents the scalar transport with similar terms as equations (3.3) and (3.4). The above equations neglect momentum transfer term that correlates wind-induced surface pressure fluctuations and wave slope.

The horizontal radiation stress terms (on the right hand-side of Equations 3.3 and 3.4) are:

$$S_{xx} = kE\left[\frac{k_x k_x}{k^2}F_{CS}F_{CC} + F_{CS}F_{CC} - F_{SS}F_{CS}\right] + \frac{k_x k_x}{k^2}\frac{c^2}{L}A_R R_{zn} \quad (3.9)$$

$$S_{xy} = S_{yx} = kE\left[\frac{k_x k_y}{k^2} F_{CS} F_{CC}\right] + \frac{k_x k_y}{k^2}\frac{c^2}{L} A_R R_{zn} \tag{3.10}$$

$$S_{yy} = kE\left[\frac{k_y k_y}{k^2} F_{CS} F_{CC} + F_{CS} F_{CC} - F_{SS} F_{CS}\right] + \frac{k_y k_y}{k^2}\frac{c^2}{L} A_R R_{zn} \tag{3.11}$$

where the terms in brackets are the traditional momentum flux terms due to the waves (as shown in Mellor 2003, 2005), and we have added the last term to account for the surface roller based on Svendsen (1984) and Svendsen et al. (2002), defined with a vertical distribution as:

$$R_{zn} = \frac{R_z}{\int R_z dz}, \qquad R_z = 1 - \tanh\left(\frac{2s}{}\right)^4 \tag{3.12}$$

where, R_z vertically distributes the additional stress term due to the roller as an exponentially decaying function with depth and γ is the ratio of wave height to water depth (γ = H_s/D), H_s is the significant wave height, k is the wavenumber (k = 2π/L where L is wavelength), k_x and k_y are the wavenumber components in the x- and y-directions and c is the wave-propagation speed, computed as:

$$c = \frac{\sigma}{k} = \sqrt{\frac{g}{k}\tanh kD} \tag{3.13}$$

where σ is the wave frequency ($\sigma = 2\pi/T$ where T is wave period). The roller area (A_R) is obtained directly from the wave model or computed from Svendsen (1984) as:

$$A_R = \frac{\alpha}{\sqrt{2}} H_s L Q_b \tag{3.14}$$

where α is a parameter with value 0.06, and Q_b is the fraction of breaking waves.

The vertical radiation-stress terms (last term on the right hand-side of Eqs. 3.3 and 3.4) are:

$$S_{px} = (F_{CC} - F_{SS})\left[\frac{F_{SS}}{2}\frac{\partial E}{\partial x} + F_{CS}(1+s)E\frac{\partial (kD)}{\partial x} - EF_{SS}\coth(kD)\frac{\partial (kD)}{\partial x}\right] \tag{3.15}$$

$$S_{py} = (F_{CC} - F_{SS})\left[\frac{F_{SS}}{2}\frac{\partial E}{\partial y} + F_{CS}(1+s)E\frac{\partial (kD)}{\partial y} - EF_{SS}\coth(kD)\frac{\partial (kD)}{\partial y}\right] \tag{3.16}$$

where the vertical structure functions in Equations (3.15) and (3.16) are:

$$F_{SS} = \frac{\sinh\big(kd(1+s)\big)}{\sinh kD} \quad , \quad F_{CS} = \frac{\cosh\big(kd(1+s)\big)}{\sinh kD} \tag{3.17}$$

$$F_{SC} = \frac{\sinh\big(kd(1+s)\big)}{\cosh kD} \quad , \quad F_{CC} = \frac{\cosh\big(kd(1+s)\big)}{\cosh kD} \tag{3.18}$$

and $E = \rho g H_s^2/16$ is the wave energy. These terms provide in the momentum equations wave forcing with a vertical structure that decays exponentially with depth.

The momentum expressions derived by Mellor (2003, 2005) yield equations with a mean velocity that is consistent with a Lagrangian reference frame. The Lagrangian and Eulerian reference frames are related by the Stokes velocities u_s and v_s in the x- and y-directions, computed as:

$$u_s = \frac{2k_x}{c}\frac{\cosh 2kD(1+s)}{\sinh 2kD}\left(E + \frac{DgA_R}{L}\right) \tag{3.19}$$

$$v_s = \frac{2k_y}{c}\frac{\cosh 2kD(1+s)}{\sinh 2kD}\left(E + \frac{DgA_R}{L}\right) \tag{3.20}$$

where the last terms in the parentheses are the roller contributions. Stokes velocities are subtracted from Lagrangian velocities to maintain a consistent Eulerian reference frame for the entire model dynamics.

The bottom boundary layer (BBL) is important for sediment transport formulations because bottom stress determines the transport rate for bedload and the re-suspension rate for suspended sediment. BBL determines the stress exerted on the flow by the bottom, which is used in the Reynolds-averaged Navier-Stokes equations as boundary conditions for momentum in the x and y directions

$$K_M \frac{\partial u}{\partial s} = \tau_{bx} \, , \quad K_M \frac{\partial v}{\partial s} = \tau_{by} \tag{3.42}$$

ROMS implements two methods for representing BBL processes: (a) simple drag-coefficient expressions, and (b) complex formulations to represent wave-current interactions over a moveable bed. The drag-coefficient methods implement formulae for linear bottom friction, quadratic bottom friction, or a logarithmic profile. The other, more complex methods implement some of the many wave–current BBL models (e.g., Jonsson and Carlsen, 1976; Smith, 1977; Grant and Madsen, 1979; Madsen, 1994; Styles and Glenn, 2000) and couple them with calculations of bottom roughness. ROMS offers three methods that implement slightly different combinations of algorithms for the wave–current interactions and moveable bed roughness. The first method (sg_bbl) is based on wave current algorithm and the ripple

geometry and movable bed roughness of Styles and Glenn (2002); the second method (mb_bbl) uses efficient wave-current BBL computations developed by Soulsby (1995) in combination with sediment and bedform roughness estimates; the third method (ssw_bbl) implements either the wave-current BBL model of Madsen (1994) or Styles and Glenn (2000), the differences in approach among these routines are small, but they can produce significantly different results. In the present research, the ssw_bbl method is implemented along with moveable bed routines.

The BBL parameterisation implemented in ROMS requires inputs of velocities u and v at reference elevation z_r, representative wave-orbital velocity amplitude u_b, wave period T, and wave-propagation direction θ (degrees, in nautical convention). The wave parameters may be the output of a wave model such as SWAN or simpler calculations based on specified surface wave parameters and should represent the full spectrum of motion near the bed. Moreover, the BBL models require bottom sediment characteristics (median grain diameter D_{50}, mean sediment density ρ_s, and representative settling velocity w_s); these are based on the composition of the uppermost active layer of the bed sediment during the previous time step.

Ripple height n_r and wavelength λ_r are calculated using information from the previous time step and the Malarkey and Davies (2003) implementation of the Wiberg and Harris (1994) formulation, which is valid for wave dominated conditions. They approximate ripple wavelength as $535D_{50}$ and ripple steepness as:

$$\frac{n_r}{\lambda_r} = exp\left[-0.095\left(ln\left(\frac{d_0}{n_r}\right)\right)^2 + 0.442\left(ln\left(\frac{d_0}{n_r}\right)\right) - 2.28\right] \tag{3.43}$$

where $d_0 = u_b T/\pi$ is the wave orbital diameter.

Roughness lengths associated with grain roughness z_{0N}, sediment transport z_{0ST}, and bedform roughness length (ripples) z_{0BF} are estimated as:

$$z_{ON} = 2.5D_{50}/30\,, \quad z_{OST} = \alpha D_{50} a_1 \frac{T_*}{1+a_2 T_*}\,, \quad z_{OBF} = a_r \eta_r^2/\lambda_r \tag{3.44}$$

where the sediment-transport coefficients are $\alpha = 0.056$, $a_1 = 0.068$, and $a_2 = 0.0204\ln(100D_{50}^2) + 0.0719\ln(100D_{50})$ with the bedform roughness D_{50} expressed in meters, $a_r = 0.267$ is a coefficient suggested by Nielsen (1992). The roughness lengths are additive, so subsequent BBL calculations use $z_0 = \max[z_{0N} + z_{0ST} + z_{0BF},\ z_{0MIN}]$, where $z_{0MIN} = 5e^{-5}\ m.$ and allows setting a lower limit on bottom drag.

The pure currents and pure wave limits are used as initial estimates for calculations towards consistent profiles for eddy viscosity and velocity between z0 and zr, using either the model of Madsen (1994) or Styles and Glenn (2000). Both of these models assume eddy viscosity profiles;

scaled by $u_{*wc} = \sqrt{\tau_{wc}}$ in the wave-boundary layer (WBL) and $u_{*c} = \sqrt{\tau_b}$ in the current boundary layer, calculated as:

$$K_M = \begin{cases} ku_{*wc}z, & z < \delta_{wbl} \\ ku_{*c}z, & z > \delta_{wbl} \end{cases} \quad (3.45)$$

where δ_{wbl} is the thickness of the WBL, which scales as $u_{*wc}T/(2\pi)$. τ_{wc} represents the maximum vector sum of wave- and current-induced stress, but the τ_b is influenced by the elevated eddy viscosity in the WBL, and must be determined through an iterative process. The parameter τ_b is the mean bed shear stress over many wave periods and is used as the bottom-boundary condition in the momentum equations, and τ_{wc} is the maximum instantaneous stress exerted over the bottom by representative waves and currents. These stresses directly influence flow near the bottom and act as agents for sediment re-suspension and bedload transport.

B.4 Wave-Ocean Models Coupling

The spectral wave model SWAN and the ocean circulation model ROMS were used to form a fully two-way coupled modelling system. The coupled system is aimed to better represent the non-linear interactions such as the wave-current interaction, from two independent models. In the ocean model, the wave fields are used to compute forcing in the form of radiation stress gradients that allow wave-driven flows, to compute Stokes velocities, to provide correct mass-flux transport and to compute wave-enhanced bottom stresses. The wave model receives varying water levels, changes in bathymetry and bottom roughness (to simulate morphological variations due to sediment transport on the sea floor), and ocean currents. The ocean surface currents affect the wave action in two ways. One way is that the source term will use the 10 m wind speed modified by the local current thereby modifying the wind stress. A second way is to use the modified group velocities which in turn effects the wave number to allow current-induced refraction.

B.5 Metocean Boundary Forcing

The boundary forcing for the set of models consist of tidal data, oceanic background currents, wave spectra and atmospheric forcing.

The tidal constituents are extracted from the Oregon State University TOPEX/Poseidon Global Inverse Solution tidal model (TPXO9.1). This is the current version of a global model of ocean tides, which best-fits, in a least-squares sense, the Laplace Tidal Equations and along track averaged data from TOPEX/Poseidon and Jason (on TOPEX/Poseidon tracks since 2002) obtained from OTIS (Oregon State University Tidal Inversion Software). Tides are provided as complex amplitudes of earth-relative sea-surface elevation for eight primary (M2, S2, N2, K2, K1, O1, P1, Q1) harmonic constituents.

TPXO9.1-atlas is a 1/30° resolution fully global solution that combines a basic global solution (TPXO9, obtained at 1/6 resolution) and a series of over 30 high resolution (HR) regional

assimilation solutions incorporated to increase resolution in coastal areas and shallow seas. The base global solution has a resolution of 1/6°, with bathymetry for the dynamical model derived from the GEBCO 1′ database (GEBCO Digital Atlas, 2003) with some adjustments around Antarctica south of 57°S. Regional solutions were obtained with a resolution of 1/30° for 33 rectangular areas, including all major enclosed or semi-enclosed seas and all the coastal areas around the world. Higher-resolution local bathymetry was used wherever possible, and all available T/P-Jason and interleaved data were assimilated. At high latitudes, or in shallow areas with sparse T/P coverage, ERS/Envisat data were also used for lunar tides. Additional coastal tide gauges were used in some regional solutions to improve estimates in local bays. The regional solutions were patched into the global TPXO8 base solution, keeping higher resolution in coastal/shallow areas and using a weighted average of regional and global solutions over a narrow strip for a smooth transition to the global model in the open ocean.

Background ocean currents, temperature, salinity and water level were taken from the so-called global HYCOM-NCODA system. The HYCOM consortium is a multi-institutional effort sponsored by the National Ocean Partnership Program (NOPP), as part of the U. S. Global Ocean Data Assimilation Experiment (GODAE), to develop and evaluate a data-assimilative hybrid isopycnal-sigma-pressure (generalized) coordinate ocean model (called HYbrid Coordinate Ocean Model or HYCOM). The GODAE objectives are the three-dimensional depiction of the ocean state at fine resolution in real time, the provision of boundary conditions for coastal and regional models, and the provision of oceanic boundary conditions for a global coupled ocean-atmosphere prediction model. The HYCOM-NCODA service is a global nowcast-forecast system developed by the HYCOM consortium. It has a 1/12° equatorial resolution and latitudinal resolution of 1/12° cos(lat) or approximately 7 km with 32 vertical levels. It is run in real time at the Naval Oceanographic Office (NAVOCEANO) Major Shared Resource Center using operational computer time. It uses atmospheric forcing from the NAVy Global Environmental Model (NAVGEM). Data assimilation is performed using the Navy Coupled Ocean Data Assimilation (NCODA) system. HYCOM reanalysis are available from 1992 to 2012. From 2012 to the present only global analysis are available.

The open boundary conditions for the SWAN model were taken from the Fugro Global Wave Database. This was produced by using an implementation of a WAVEWATCH III model for the global ocean with a resolution of 50 km. Spectral data was recorded for a period of 35 years. The global model was validated against satellite altimetry data taken from 9 different satellites.

Atmospheric data were sourced from the hindcast data from the American National Centers for Environmental Prediction (NCEP) Climate Forecast System Reanalysis. CFSR was designed and executed as a global, high resolution, coupled atmosphere-ocean-land system to provide the best estimate of the state of these coupled domains. CFSR hindcast data are available at 0.312° grid resolution and cover the period from 1979 to 2010 in 6-hourly intervals. From 01 January 2011 CFSR has been extended by NCEP's Climate Forecast System Version 2 (CFSv2)

operational model. The data produced by CFSv2 can be considered as a seamless extension to CFSR.

B.6 Model Setup

The wave model was run and coupled in the grid domain (see Figure 3.1) with a 362x314 grid domain, horizontal resolution is about 500 meters in x and y directions; wave boundary conditions are imposed at the four boundaries, where they come from the spectral global wave conditions; wind fields are every 3 hours for the entire domain; the wave model runs in third-generation mode for wind-input, quadruplet interactions and white capping. The bottom friction is given by the Madsen et al. (1988) approximation, and it varies over the computational region and is computed within ROMS model; the triad wave-wave interaction is also activated; numerical propagations uses the BSBT method; the computational spectral grid is defined for swell winds with a resolution of 10 degrees that is enough for the spectral directional resolution, the grid resolution interval in frequency-space is 46, even, the directional spread of the waves (directional spreading coefficient), that drives the incoming wave directions, is set as 36 for a reasonably surfing swell, discrete frequencies varies between the minimum 0.03 and the maximum 2.5 frequencies.

The wave model exports fields of wave heights, wave period, wave directions, wave particle velocities at the top and bottom, and forces as radiation stresses for the wave contribution in the circulation model. Fields of water elevation, water depth and velocity currents, as well as, bottom friction come from the two-way coupled circulation model ROMS.

The ROMS model was run in baroclinic mode with 8 terrain-following (sigma) layers in the vertical; the numerical grid has 362 grid cells in the longitude direction, which extends from 71.70W to 69.54W. Along the latitude direction the grid has 314 grid cells and the domain extends from 40.5N to 41.91N. The coordinates for both, the wave and flow models are in curvilinear coordinates. The Nikuradse bottom roughness is considered constant over the entire simulation with a value of 0.05 m. The vertical turbulent mixing scheme used is the Generic Length-Scale model (Warner et al, 2008), parameterised as κ-ε (κ-ε model is the most commonly used of all the turbulence models. It is classified as a two-equation model; this denotes the fact that the transport equation is solved for two turbulent quantities κ and ε). Salinity and temperature remain constant, S_o= 30 psu and T_o = 10 Celsius.

Boundary conditions for tidal forcing were derived from the OTIS model (Egbert and Erofeeva, 2002; Padman and Erofeeva, 2004), tidal elevations and tidal currents were interpolated to the boundaries of the computational grid in ROMS.

The available boundary conditions within the flow model ROMS are defined as follows: for the barotropic currents the Flather boundary condition (Flather, 1976) is set, this boundary condition allows the free propagation of the barotropic currents through the four boundaries. For the free surface boundary the Chapman boundary condition (Chapman, 1985) is applied because it allows and includes wave propagation and also gives stability for the gravity wave conditions. In general, most of the physical default parameters were held constant (e.g.

harmonic/biharmonic horizontal and vertical mixing, turbulent closure parameters, surface turbulent kinetic energy flux, momentum stress, density and linear equation of state parameters).

To perform the wave-current interaction, data exchange between the wave and flow models is necessary. The first requirement to exchange data is to agree on the units of the parameters (e.g. m/s^2 or N/m^2) and the exact definition (e.g. H_{m0} or H_{rms}). Then, a central grid to interpolate between grids is adopted. Generally, the flow model grid is chosen as the central grid, which is the same for transports and morphological changes.

In ROMS the baroclinic time step is set as 90 s and a mode-splitting ratio of 30 s. In SWAN, for this coarse grid, the time step is 1200 s. An exchange rate of data between ROMS and SWAN is every 1200 s.

The model was run for a period little over 2 years (July 1, 2018 to August 31, 2020). Model parameters were outputted at hourly intervals. Standard parameters were outputted (wave and 3d current fields).

Attachment C

Sediment Plume Dispersion Model

C.1 General Methodology

To predict the distribution of sediment that are discharged into the environment, Fugro developed a numerical model capable of simulating their dispersion from the release to the moment they are deposited on the seabed. The dispersion of the sediment is estimated using numerical modelling, by releasing lumps of material at regular time intervals and variable locations during the release period. The model allows for sediment dispersion studies with a high flexibility, considering three-dimensional current velocity and density forcing on variable topography. Following the best practices, the model considers two consecutive stages.

C.1.1 First Stage: Convective Descent/Ascend in the Near-Field Zone

The sediment discharge consists in a jet of material, characterised with some initial buoyancy and assumed to be well-mixed. The equations of conservation of mass, momentum and buoyancy are solved to simulate the plume trajectory. As the jet descends or ascends, it entrains the ambient fluid and grows in diameter, with its density and velocity approaching those of the ambient fluid (Khondaker 2000). While the jet density approaches the ambient density, its vertical velocity decreases, allowing the sediment to settle out and leave the plume. When the settling velocity associated with a class of solid particle exceeds the descent or ascend velocity of the jet, it falls out of the plume and continues to the second stage: far-field dispersion and deposition. The convective stage for the plume ends when:

- The plume reaches the surface or the seafloor. Every class of solid particles that is still present within the plume is released from the plume and continues to the second stage;
- All the classes of solid particles have left the plume.

C.1.2 Second stage: Far-Field Dispersion and Deposition.

After they are released from the plume, the sediment dispersion is governed by an advection equation of the form:

$$\frac{d\vec{x}}{dt} = \vec{v}\,,$$

where t is the time elapsed since the release of the lump, $\vec{x}$ is the position of the centre of mass of the lump and $\vec{v}$ its velocity, which can be decomposed into:

$$\vec{v} = \overrightarrow{v_a} + \overrightarrow{v_s} + \overrightarrow{v_r}.$$

The first term corresponds to the two-dimensional advection by the prevailing ambient current velocity $\overrightarrow{v_a}$. The fall velocity $\overrightarrow{v_s}$ points downwards and is estimated using the formula from CERC (1984) based on the sediment particle sizes. Following Tanaka (1994), diffusion is accounted through a random motion of associated velocity:

$$\overrightarrow{v_r} = \left[R\left(\sqrt{\frac{2\kappa_h}{\Delta t}}\right) \quad R\left(\sqrt{\frac{2\kappa_h}{\Delta t}}\right) \quad R\left(\sqrt{\frac{2\kappa_v}{\Delta t}}\right) \right]',$$

where $R(\sigma)$ is a random number obtained from a normal distribution of standard deviation σ, while Δt is the time step used for the numerical integration in time and $\vec{\kappa} = (\kappa_h, \kappa_h, \kappa_v)$ is the diffusivity vector. The advection equation is then integrated in time until the lump settles on the sea bottom.

A certain volume of soil corresponds to each lump. A Gaussian diffusion operator is used to deduce the local sediment turbidity level or seabed deposit thickness from the location of the lump's centre of mass and the travel time.

The released volume is distributed in a certain number of sediment lumps, each lump representing an equal fraction of the total volume for each class of sediment. A lump of each class of sediment is released at regular time intervals and locations during the planned time of the dredging or drilling operations.

The model allows for sediment dispersion studies with high flexibility that use available data as completely as possible:

- Depth-averaged or three-dimensional current velocity forcing
- Flat or variable topography
- In-situ or estimated grain size distributions
- Variable release schedule, path, direction, and height